Journal of the Mechanics and Physics of Solids 138 (2020) 103897

Contents lists available at ScienceDirect

Journal of the Mechanics and Physics of Solids

journal homepage: www.elsevier.com/locate/jmps

Continuum homogenisation of stochastic comminution with grainsize fabric

Eric Huang, Benjy Marks, Itai Einav*

School of Civil Engineering, The University of Sydney, NSW 2006, Australia

ARTICLE INFO

Article history:
Received 4 November 2019
Revised 21 January 2020
Accepted 4 February 2020
Available online 12 February 2020

Keywords:
Granular matter
Comminution
Grain crushing
Stochastic processes
Heterarchy
Homogenisation
Breakage

ABSTRACT

Comminution is the process of grainsize reduction due to grain crushing, which is common in both natural and industrial problems that involve brittle granular media. Grain crushing is a stochastic process, where the strength of individual grains is determined both by their own size and mineralogy, and the local arrangement of their neighbouring particles, here termed *grainsize fabric*. The relationship between these effects was described previously using a stochastic lattice model of comminution, whose most general form further includes segregation and mixing. While the stochastic segregation and mixing dynamics have simple analogous differential equations for describing the equivalent continuum behaviour, until now the stochastic comminution dynamics has lacked a smooth representation. Here we resolve this gap by developing a homogeneous continuum model that is based on the same stochastic physics. We show that the new model yields the same results as the stochastic lattice model in the limit of indefinitely large lattices. Given a time varying stress state, the model describes the time-evolution of the grainsize distribution by representing the state of the system in terms of a two-dimensional joint distribution over grainsize and local-average grainsize. The model has a scalable numerical implementation with a simple deterministic rule for time-evolution.

1. Introduction

The behaviour of granular media depends on the relative proportions of the constituent grain sizes, the *grainsize distribution*. Understanding how this grainsize distribution evolves in granular media is important as they control many phenomena in nature and industry. In particular, comminution is the process of grainsize reduction due to grain crushing, which critically determines the motion of earthquake fault gouges and the energetics of grinders and mills in mineral processing. In confined granular media, comminution starts when the local stress inside a grain exceeds its crushing strength. After many successive crushing events, this can significantly change the grainsize distribution of the material. The local stress inside a grain depends on its interactions with its neighbouring grains, and their specific configuration encodes a "memory" of the medium's history. We define the local organisation of grainsizes within a representative volume element as the *grainsize fabric*, and will show both how this measure is key to modelling the comminution process, and how it affects the evolution of the grainsize distribution. In this paper, we eventually develop a simplified model where the grainsize fabric is represented by a two-dimensional probability density function, which is different to the tensor-based representations of conventional

* Corresponding author.
E-mail address: itai.einav@sydney.edu.au (I. Einav).

https://doi.org/10.1016/j.jmps.2020.103897
0022-5096/

contact and force fabrics (e.g., Kruyt, 2012; Oda, 1982), both in terms of the mathematical structure and physical role. The continuum representation of materials such as Newtonian fluids and elastic solids has been widely used for many practical applications, thanks to the development of efficient continuum mechanics numerical solvers such as the finite element method. For comminution processing, however, despite its prevalence a mathematical continuum description has not been developed. Successful comminution models have been produced on the basis of breakage mechanics theory (Einav, 2007a; 2007b; Zhang and Buscarnera, 2017) for closed systems without size-dependent advection from the neighbourhood. However, these are not appropriate for open systems where material can advect in space, as the grainsize dynamics further depend on segregation and mixing.

Recently we have partially resolved this issue of coupled grainsize dynamics by advancing a different modelling philosophy, initially through the development of a novel stochastic lattice model (Marks and Einav, 2015; 2017). We first showed that this model predicts grainsize dynamics that agree well with open-system grainsize dynamics from field data (Marks and Einav, 2015) and closed-system comminution dynamics from laboratory data for different initial grainsize distributions (Guida et al., 2020). Additionally, we were able to derive the macroscopic partial differential equations that correspond to the smooth limit of the stochastic lattice model for segregation and mixing, in the absence of comminution. However, the homogenisation of the comminution part of the model was left behind, as it was deemed to be more difficult to derive, since it relied on information about the relative arrangement of particles below the resolution of a representative volume element. Here, we resolve exactly this gap, as we develop the deterministic homogenised continuum description of the comminution part of the stochastic lattice model.

The newly developed continuum model encodes the internal arrangement of grains in a two-dimensional probability distribution function over grainsize and neighbourhood grainsize. In this two-dimensional space, there is a zone of destruction that grows with the externally applied stress such that anything within it will be crushed. The experimentally measurable marginal grainsize distribution is recovered by summing over the neighbourhood grainsize axis. In this way, we show that the new continuum model explicitly predicts smooth grainsize dynamics during confined comminution, which matches the experimentally validated dynamics (Guida et al., 2020) obtained by the stochastic model at the limit of large specimen sizes. In the future this model could be combined with the deterministic homogenised continuum descriptions of the segregation and the mixing. In this way we will finally be able to use continuum mechanics to describe the diverse problems of comminution in open systems, including complex geophysical phenomena such as earthquake fault gouges, rock flows, landslides and avalanches, as well as industrial milling and grinding operations.

1.1. Existing models of comminution

Power law grain size distributions are often empirically observed in earthquake fault gouges (An and Sammis, 1994; Hattori and Yamamoto, 1999; Marone and Scholz, 1989; Sammis et al., 1987) and crushed ice (Palmer and Sanderson, 1991). This is very different from other processes such as the wind-deposition of aeolian sands (Barndorff-Nielsen, 1977) where exponentially decreasing distributions for the logarithm of particle size have been observed. Consequently many fractal-inspired models (McDowell et al., 1996; Turcotte, 1989) predicting power-law distributions in confined comminution are among a diverse spectrum of theoretical explanations. Aranson and Tsimring (2006), Grady and Kipp (1985)

Meanwhile, log-normal distributions have been observed in comminution with thorough mixing. This was first explained by Kolmogorov (1941) who showed that independent grain crushing events asymptotically lead to a log-normal distribution by the central limit theorem. Halmos solved a similar problem in probability theory (Halmos, 1944) and Epstein (1947) constructed a statistical model for the crushing of grains in terms of particle size distributions $F_n(x)$ indexed by discrete crushing events $n = 0, 1, 2, \ldots$ and explicitly proved the conditions for log-normality to be that the probability of crushing is independent of the sizes of other grains and that the fragment distribution is the same for all events. Further refinements along these lines were made in Dacey and Krumbein (1979) where a selection rule for which grain to break is added. Unfortunately grain crushing is not independent from the properties of neighbouring grains in general, especially in confined systems when dense particles are constantly in contact with one another. Crushing two uniformly graded samples of different grainsizes and mixing them together yields a completely different grainsize distribution to first mixing them together and then crushing.

However, grainsize distributions observed in nature are rarely either log-normal or power-law, so breakage mechanics (Einav, 2007a; 2007b) describes closed comminution as a continuous thermodynamic process from an initial distribution state. Before the stochastic lattice model (Marks and Einav, 2017) was proposed, there were limited descriptions of how the grainsize distributions should evolve as a function of applied stress and initial grainsize distribution.

Many alternative models have been proposed, including mineral liberation models with population balance equations (Ramkrishna, 2000) and batch comminution (King and Schneider, 1998). Another probabilistic liberation model has been developed (Gay, 2004) where entropy (Espanol, 2004) plays a central role. However, these models do not explicitly predict the time-evolution of grainsize distributions in confined systems with sustained particle contacts.

These models also do not account for the internal rearrangement of neighbouring grains constituting the *grainsize fabric* of the material, which is very important for comminution since two samples of granular matter with the same initial grainsize distribution but different internal rearrangement of particles will have significantly different behaviour. For example, crushing a sample up to some stress and then remixing the sample before further crushing may be easier than crushing the soil without remixing (Lrincz et al., 2005).

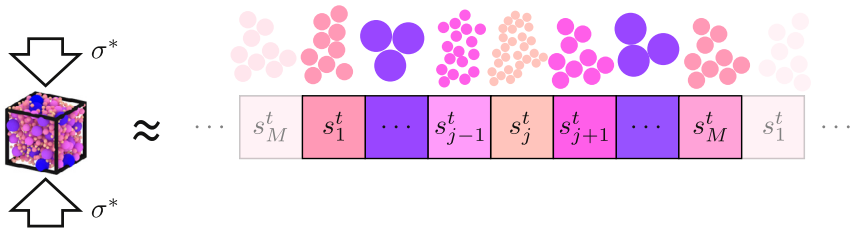

Fig. 1. The mapping from a volume of granular material to a lattice in the stochastic lattice model. Each representative volume element maps to a 1D array $\mathbf{s}^t = \left(s^t_1, s^t_2, \ldots, s^t_M\right)$ with periodic boundary conditions. The lattice evolves according to a simple set of rules under comminution by an externally applied stress ratio σ^*.

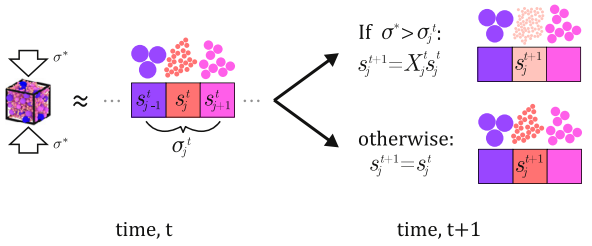

Fig. 2. The comminution rule of the stochastic lattice model for a cell s^t_j. When the applied stress ratio $\sigma^*(t)$ exceeds some critical stress $\sigma^t_j = \sigma\left(s^t_{j-1}, s^t_j, s^t_{j+1}\right)$, the new grainsize at the next time step is reduced by a factor of X^t_j which are independent identically distributed random variables following some given fragment distribution. Otherwise, the cell is left untouched. The same rule and σ^* applies for all M cells in the lattice.

2. Stochastic lattice model

The *stochastic lattice model* or *heterarchal multi-scale model* in Marks and Einav (2015, 2017) is the starting point of our comminution model as it elegantly captures segregation, mixing and comminution in a unified lattice framework. The full model describes a lattice state $\mathbf{s}^t$ with elements $s^t_{i,j}$ that evolve in discrete time t. Here, the t-superscripts are time labels and not exponents, the index i discretises space into representative volume elements holding statistically significant samples of grains, while $j \in \{1, 2, \ldots, M\}$ for some large M is an internal grainsize coordinate for that representative volume element i as depicted in Fig. 1. Any properties predicted should converge in the limit of large M. The greatest appeal of this model is its simplicity and consistency in covering a large range of granular phenomena. Since the packing of granular media greatly depends on the grainsize distribution (Göncü et al., 2010; Yu and Standish, 1988), another advantage of this model is its ability to provide crucial information on the densification of granular materials due to comminution (Guida et al., 2020).

We consider the comminution rule for just a single representative volume element by dropping the space index i and considering only the grainsize index j as depicted in Fig. 2. For each cell j, there is a grainsize s^t_j that represents the average grainsize of a collection of grains in that volume element. Every cell in the lattice represents a *collection* of grains with a fixed total mass that remains constant in time such that mass conservation naturally arises even as its *average* grainsize s^t_j changes over time. Every cell is subjected to the same external stress ratio σ^*, which is the ratio of the applied stress to the minimum stress needed to induce first crushing. Although not considered in this paper, the compaction and densification may in principle be computed from the state of the grainsize distribution, as discussed in Guida et al. (2020). This is a proxy for the maximum tensile stress experienced by any grain and may in general vary with time to follow an applied loading pattern. The grainsize of each cell evolves in time according to

$$s^{t+1}_j = \begin{cases} X^t_j s^t_j & \text{if } \sigma^* \geq \sigma^t_j\left(s_{j-1}, s_j, s_{j+1}\right) \\ s^t_j & \text{otherwise,} \end{cases} \tag{1}$$

where X^t_j is a *grainsize reduction factor* between 0 and 1 that is randomly drawn from a fragment distribution and $\sigma^t_j = \sigma\left(s^t_{j-1}, s^t_j, s^t_{j+1}\right)$ is the maximum stress ratio a cell could take without crushing. Based on physical arguments about microscopic packing arrangements and grain strength, this function was proposed in Marks and Einav (2017) to take the form

$$\sigma\left(s^t_{j-1}, s^t_j, s^t_{j+1}\right) = \left(\frac{s^t_j}{s_{\max}}\right)^{-3/w} \exp\left[\frac{\log\left(s^t_j / \bar{s}^t_j\right)^2}{2n^2}\right] \tag{2}$$

where $\bar{s}^t_j := (s^t_{j-1} + s^t_{j+1})/2$ is the average neighbourhood grainsize, $s_{\max}$ is some fixed maximum grainsize, w is a Weibull parameter and n is some dimensionless scaling parameter. That this depends only on the grainsizes of itself s^t_j and of its nearest neighbours s^t_{j-1}, s^t_{j+1}, reflects that here each grain in a granular material only interacts with its nearest neighbours.

The state of the system is an M-dimensional positive real vector $\mathbf{s}^t = (s_1^t, s_2^t, \ldots, s_M^t) \in \mathbb{R}^M$ storing the grainsize of each cell at time $t \in \mathbb{N}$, where $\mathbb{N} = \{0, 1, 2, 3 \ldots\}$ are the natural numbers. The evolutionary path of the system is thus represented by an ordered set of states $\{\mathbf{s}^t\}_{t\in\mathbb{N}}$ enumerated by time $t \in \mathbb{N}$. This is different from continuous-time-evolution in assuming that crushing events occur on a single time step and is justified if crushing events are fast compared to the time scale of stress changes.

Unless noted otherwise from here onwards, uppercase symbols will be used to denote random variables while lowercase letters will be used for non-random variables. Boldface letters will be used to denote vector quantities. Calligraphic fonts will be used to denote sets and probability distribution objects.

The stochastic lattice model may be formulated as a *stochastic process* $\left\{\mathbf{S}^t\right\}_{t\in\mathbb{N}}$, where the state vectors $\mathbf{s}^t = \left(s_1^t, s_2^t, \ldots, s_M^t\right)$ themselves are promoted to vector-valued (multi-variate) *random variables* $\mathbf{S}^t = \left(S_1^t, S_2^t, \ldots, S_M^t\right)$, which follow some high-dimensional joint probability distribution that accounts for correlations between each variable (Castiglione et al., 2008; Sethna, 2011).

Under an externally applied stress ratio $\sigma^*(t)$, the jth cell crushes if the applied load ratio σ^* exceeds its critical stress ratio σ_j^t. Hence time-evolution is completely characterised by a stress function $\sigma : \mathbb{R}^3 \to \mathbb{R}$ that maps the three real grainsizes $s_{j-1}^t, s_j^t, s_{j+1}^t$ in the neighbourhood $(j-1, j, j+1)$ about each j to a real critical stress ratio given by $\sigma_j^t = \sigma(s_{j-1}^t, s_j^t, s_{j+1}^t)$. For simplicity, we assume periodic boundary conditions such that the neighbourhood of cell 1 is (M, 1, 2) and the neighbourhood of cell M is $(M-1, M, 1)$.

In this work, we are only interested in the *event-driven* or *quasi-static regime* where the stress function $\sigma^*(t)$ changes very slowly compared to crushing events which occur almost instantaneously relative to the time scale of changes in applied stress and equilibration. Thus at most only a single cell will crush upon any time step, which is why t may be discrete while fully describing the dynamics.

The grainsize reduction factors $X_j^t \sim \mathcal{F}_X$ in the time-evolution rule (1) are *independent identically distributed* random variables with some probability distribution $\mathcal{F}_X$. Here ~ denotes the random variable X_j^t being distributed according to the probability distribution $\mathcal{F}_X$ termed the *fragment distribution*. Its exact form does necessarily affect the mathematical structure of the model itself but the most physically well-motivated candidate is a Weibull distribution as discussed in Section 2.1.

2.1. Fragment distribution

The grainsize reduction factors X_j^t follow the same fragment distribution $\mathcal{F}_X$, which is described by some probability density function $\rho_X(x)$ with *support* over the interval (0,1]. Meanwhile, the probability distribution $\mathcal{F}$ of the log-space grainsize reduction factor $R_j^t = \log X_j^t$ is described by a probability density function $f(r)$ with support over the closed interval $(-\infty, 0]$.

The distribution of fragment sizes from a single grain undergoing brittle fracture was first theoretically investigated (Gilvarry, 1961) on the basis of Griffith crack propagation theory (Griffith, 1921) with the assumption that fracture starts from the independent activation of randomly distributed flaws in the bulk which propagate to the surface. The resulting theoretical fragment distribution is a Weibull distribution Weibull (1951) defined by two positive parameters λ, κ in a probability density function of the form

$$\rho_X(x) = \frac{\frac{\kappa}{\lambda}\left(\frac{x}{\lambda}\right)^{\kappa-1} e^{-(x/\lambda)^\kappa}}{1 - e^{-\lambda^{-\kappa}}} \tag{3}$$

with support over (0,1].

Discrete element simulations (McDowell and Harireche, 2002) of a single crushing grain produce fragment size distributions consistent with this prediction. While discrete element methods may in principle be applied to small quantities of granular matter (Miao et al., 2017; Morrison and Cleary, 2004), these algorithms are computationally expensive to scale to bulk quantities of macroscopic granular matter necessary for a statistical description of grainsize evolution.

For the special case $\lambda = 1$ and $\kappa = 1$, the probability density for each transformed variable R_j^t is

$$f(r) = \frac{\exp(r - e^r)}{1 - e^{-1}}, \tag{4}$$

with support over $(-\infty, 0]$. We shall use this for numerical examples.

3. Interpretation as a Markovian discrete-time stochastic process

A *joint probability distribution* describes the probability distribution of two or more variables. If the variables are independent, then the joint probability density function is their product, but this is usually not the case if they are *correlated*. The joint probability distribution for $\boldsymbol{S}^t$ is uniquely described by a cumulative distribution function

$$F_{\mathbf{S}}^t(s_1, s_2, \ldots, s_M) := \mathbb{P}\left[S_1^t \le s_1, S_2^t \le s_2, \ldots, S_M^t \le s_M\right], \tag{5}$$

where we have used the notation $\mathbb{P}[A]$ to denote the probability of an event A. Since this function contains all information about the random variable $\boldsymbol{S}^t$, a rule that gives $F_{\mathbf{S}}^{t+1}$ given $F_{\mathbf{S}}^t$ is a deterministic formulation that describes the time-evolution from an initial distribution $F_{\mathbf{S}}^0$ to a final distribution $F_{\mathbf{S}}^t$.

Since this time-evolution rule does not depend on the state of the system at any times before the present time step, this is a *Markovian process* with no memory of its previous history beyond the present state $\boldsymbol{S}^t$.

3.1. Crush zone

For each cell j and applied stress ratio σ^*, it is useful to define a *crush zone* $\mathcal{A}_j^{\sigma^*}$ as a region in state space $\mathbb{R}^M$ where cell j is crushing.

$$\mathcal{A}_j^{\sigma^*} := \{\mathbf{s} \in \mathbb{R}^M \mid \sigma^* \geq \sigma\left(s_{j-1}, s_j, s_{j+1}\right)\}. \tag{6}$$

Its set complement $\mathcal{A}_j^{\bar{\sigma}^*} = \mathbb{R}^M \setminus \mathcal{A}_j^{\sigma^*}$ is the *non-crushing zone* for cell j.

The *indicator function* $\mathbf{1}_{\mathcal{A}} : \mathbb{R}^M \to \{0, 1\}$ of a subset $\mathcal{A} \subseteq \mathbb{R}^M$ is defined by

$$\mathbf{1}_{\mathcal{A}}(\mathbf{s}) := \begin{cases} 1 & \text{if } \mathbf{s} \in \mathcal{A} \\ 0 & \text{if } \mathbf{s} \notin \mathcal{A}, \end{cases} \tag{7}$$

in terms of which the time-evolution rule may be linearly written as

$$S_j^{t+1} = X_j^t S_j^t \mathbf{1}_{\mathcal{A}_j^{\sigma^*}}\left(\mathbf{S}^t\right) + S_j^t \mathbf{1}_{\mathcal{A}_j^{\bar{\sigma}^*}}\left(\mathbf{S}^t\right). \tag{8}$$

Using the identity $\mathbf{1}_{\mathcal{S}} + \mathbf{1}_{\bar{\mathcal{S}}} = 1$, we may factorise this into

$$S_j^{t+1} = S_j^t\Big[\left(X_j^t - 1\right)\mathbf{1}_{\mathcal{A}_j^{\sigma^*}}\left(\mathbf{S}^t\right) + 1\Big]. \tag{9}$$

This is the time-evolution rule that is in the desired form for a Markovian process.

3.2. Logarithmic transformation

As the crushing reduces each grainsize S_j^t by a random factor of X_j^t to yield a new random grainsize $X_j^t S_j^t$, it is more natural to work in log-space so multiplication becomes addition. Thus we redefine the state vector random variable as $\boldsymbol{\Psi}^t = (\Psi_1^t, \Psi_2^t, \ldots, \Psi_M^t) \in \mathbb{R}^M$ whose components are $\Psi_j^t := \log S_j^t$. Kolmogorov (1941), Halmos (1944), Epstein (1947) Under these new coordinates, the multiplicative time-evolution rule (1) may be rewritten as an additive rule

$$\Psi_j^{t+1} = \begin{cases} R_j^t + \Psi_j^t & \text{if } g^* \geq g\left(\Psi_{j-1}^t, \Psi_j^t, \Psi_{j+1}^t\right) \\ \Psi_j^t & \text{otherwise,} \end{cases} \tag{10}$$

where the stress ratio σ^* and stress function $\sigma(s_{j-1}, s_j, s_{j+1})$ have been replaced by their log-space equivalents g^* and $g(\psi_{j-1}, \psi_j, \psi_{j+1})$, while the fragment reduction factors X_j^t have also been transformed into $R_j^t := \log X_j^t$ each with support over $(-\infty, 0]$.

Note that the inequality $g^* \geq g(\psi_{j-1}, \psi_j, \psi_{j+1})$ is invariant under multiplication by a positive constant, so we are free to rescale g^* and g at our convenience.

Under these new variables, the time-evolution rule may be rewritten as

$$\Psi_j^{t+1} = \Psi_j^t + R_j^t \mathbf{1}_{\mathcal{A}_j^{g^*}}(\boldsymbol{\Psi}^t) \tag{11}$$

where the crushing zone for the jth cell for some load ratio g^* has been redefined in terms of log-space coordinates as

$$\mathcal{A}_j^{g^*} := \left\{\boldsymbol{\psi} \in \mathbb{R}^M \mid g^* \geq g\left(\psi_{j-1}, \psi_j, \psi_{j+1}\right)\right\} \tag{12}$$

where $g : \mathbb{R}^3 \to \mathbb{R}$ is the log-space stress function that relates log-space grainsizes ψ_{j-1}, ψ_j and ψ_{j+1} in a neighbourhood to the critical log-space stress ratio g_j^t that will cause crushing on the jth cell. From here on, the terms grainsize and stress shall be used interchangeably with their log-space analogues.

To simplify notation, let us define the M-dimensional binary vector-valued function $\boldsymbol{\Theta} : \mathbb{R}^M \to \{0, 1\}^M$ that maps from points in ψ-space to M-dimensional binary vectors whose components are defined by $\Theta_j(\boldsymbol{\psi}) := \mathbf{1}_{\mathcal{A}_j^{g^*}}\left(\boldsymbol{\psi}\right)$ so that the time-evolution equation may be written as

$$\Psi_j^{t+1} = \Psi_j^t + R_j^t \Theta_j\left(\Psi_j^t\right). \tag{13}$$

Using the *Hadamard product* notation $\odot$ defined component-wise between two vectors as $(\boldsymbol{A} \odot \boldsymbol{B})_j := A_j B_j$, the time-evolution equation may then be neatly written in vector form

$$\boxed{\boldsymbol{\Psi}^{t+1} = \boldsymbol{\Psi}^t + \mathbf{R}^t \odot \boldsymbol{\Theta}\left(\boldsymbol{\Psi}^t\right).} \tag{14}$$

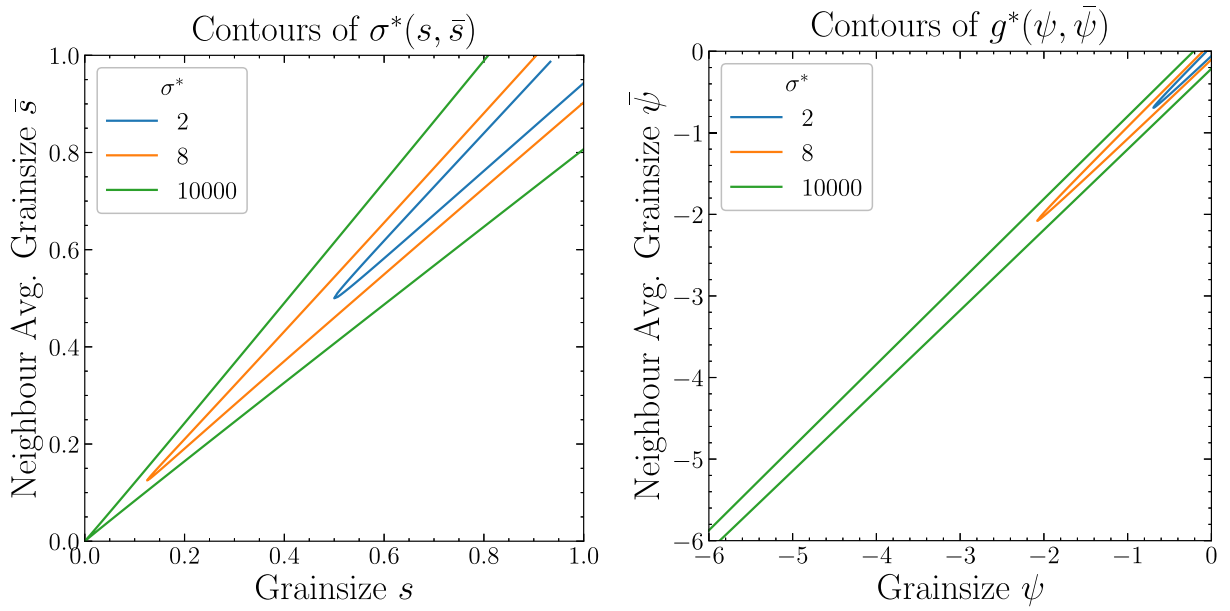

Fig. 3. Contours of the crush zone boundary $g(\psi, \bar{\psi}) = (\psi - \bar{\psi})^2 - k\psi = g^*$ for constant $k = 0.005$ and applied stress ratios $\sigma^* = 2$ (blue), $\sigma^* = 8$ (orange) and $\sigma^* = 10000$ (green) using stochastic lattice model parameters $w = 3$, $n = 0.05$, $s_{\max} = 1$ as in Marks and Einav (2017). The same contours are plotted in regular grainsize $(s, \bar{s})$ (left) and logspace grainsize $(\psi, \bar{\psi})$ (right). (For interpretation of the references to colour in this figure legend, the reader is referred to the web version of this article.)

3.3. Crushing zone geometry

The crushing criterion $\sigma^* \geq \sigma_j^t$ may be interpreted as defining a zone in the space of states where crushing will occur, whose geometry is described by Eq. (2). Moving into log-space with $\psi_j^t = \ln s_j^t$, $\bar{\psi}_j^t = \ln \bar{s}_j^t$, $k = 6n^2/w$ and $g^* = 2n^2 \ln(\sigma^*/s_{\max}^{3/w})$, the crushing criterion of Eq. (2) is

$$g^* \geq g\left(\psi_j^t, \bar{\psi}_j^t\right) \quad \text{where} \quad g(\psi, \bar{\psi}) = \left(\psi - \bar{\psi}\right)^2 - k\psi. \tag{15}$$

This quadratic form is in fact the most minimalist two-variable function that respects the symmetries of the system. For each cell j, the crush zone $\mathcal{A}_j^{g^*}$ defined in terms of a critical stress function $g(\psi_{j-1}, \psi_j, \psi_{j+1})$ encodes and characterises the stress state. Example boundaries of this form are plotted as contours in Fig. 3 using the parameterisation $\bar{\psi} = \psi \pm \sqrt{g^* + k\psi}$.

4. Reformulation for deterministic evolution of distributions

The stress function g and fragment distribution $\mathcal{F}$ uniquely specify the time-evolution of the state $\boldsymbol{\Psi}^t$ under some external load g^*. It is then natural to ask how its probability density $\rho_{\boldsymbol{\Psi}}^t(\boldsymbol{\psi})$ evolves *deterministically* over time. This is analogous to the *Fokker–Planck equations* for Brownian motion (Espanol, 2004).

For the stochastic process $\left\{\boldsymbol{\Psi}^t\right\}_{t\in\mathbb{N}}$ we have previously formulated, we derive the time-evolution of the joint probability density function $\rho_{\boldsymbol{\Psi}}^t(\boldsymbol{\psi})$ for the random state vector $\boldsymbol{\Psi}^t$ using similar ideas and techniques.

The joint *probability density function*

$$\rho_{\boldsymbol{\Psi}}^t(\boldsymbol{\psi}) := \frac{\partial^M F_{\boldsymbol{\Psi}}^t}{\partial\psi_1\,\partial\psi_2\cdots\partial\psi_M}(\boldsymbol{\psi}) \tag{16}$$

is a convenient equivalent description of the joint probability distribution for our purposes. For brevity, we will often use the notations $\rho_{\boldsymbol{\Psi}}^t(\boldsymbol{\psi})$ and $\mathbb{P}\left[\boldsymbol{\Psi}^t = \boldsymbol{\psi}\right]$ interchangeably.

4.1. Time-evolution operator

The most general form of the time-evolution rule for a discrete-time stochastic process is

$$\boldsymbol{\Psi}^{t+1} = L\left[\boldsymbol{\Psi}^t\right], \tag{17}$$

where L is a *time-evolution operator* that maps from a random variable Ψ^t at time t to its time-evolved random variable Ψ^{t+1} at time $t+1$. We may equivalently consider its induced functional operator $\mathcal{L}$ which maps distributions to distributions, with

the corresponding time-evolution rule

$$\rho_{\boldsymbol{\Psi}}^{t+1} = \mathcal{L}\left[\rho_{\boldsymbol{\Psi}}^{t}\right]. \tag{18}$$

Deriving the explicit form of this operator is the main result of this paper.

Recalling the time-evolution Eq. (14), we see by inspection that the time-evolution operator is

$$L[\boldsymbol{\Psi}] := \boldsymbol{\Psi} + \mathbf{R} \odot \boldsymbol{\Theta}(\boldsymbol{\Psi}) \tag{19}$$

where the components R_j of $\boldsymbol{R}$ are i.i.d. random variables with probability density function $f(r)$ supported over $(-\infty, 0]$,

4.2. Transition probability

Recall that the stochastic process $\left\{\boldsymbol{\Psi}^t\right\}_{t\in\mathbb{N}}$ is Markovian, so

$$\mathbb{P}\left[\boldsymbol{\Psi}^{t+1} = \boldsymbol{\psi}^{t+1} \mid \boldsymbol{\Psi}^t = \boldsymbol{\psi}^t\right] = \mathbb{P}\left[\boldsymbol{\Psi}^{t+1} = \boldsymbol{\psi}^{t+1} \mid \boldsymbol{\Psi}^0 = \boldsymbol{\psi}^0, \boldsymbol{\Psi}^1 = \boldsymbol{\psi}^1, \ldots, \boldsymbol{\Psi}^t = \boldsymbol{\psi}^t\right], \tag{20}$$

where the notation $\mathbb{P}[A|B]$ denotes the *conditional probability* of event A given event B. Hence the time-evolution operator $\mathcal{L}$ may be completely specified by a conditional probability distribution function

$$\Gamma\left[\boldsymbol{\psi}|\boldsymbol{\phi}\right] := \mathbb{P}\left[\boldsymbol{\Psi}^{t+1} = \boldsymbol{\psi} \mid \boldsymbol{\Psi}^t = \boldsymbol{\phi}\right] \tag{21}$$

that holds for all t, which we call the *transition probability function*. Its values represent the probability of a state $\boldsymbol{\phi}$ evolving into state $\boldsymbol{\psi}$ on the next time step. Recalling the form of the time-evolution equation, we proceed to explicitly evaluate

$$\Gamma\left[\boldsymbol{\psi}|\boldsymbol{\phi}\right] := \mathbb{P}\left[\boldsymbol{\Psi}^{t+1} = \boldsymbol{\psi} \mid \boldsymbol{\Psi}^t = \boldsymbol{\phi}\right] = \mathbb{P}\left[\boldsymbol{\phi} + \mathbf{R} \odot \boldsymbol{\Theta}(\boldsymbol{\phi}) = \boldsymbol{\psi}\right] \tag{22}$$

$$= \mathbb{P}\left[\mathbf{R} \odot \boldsymbol{\Theta}(\boldsymbol{\phi}) = \boldsymbol{\psi} - \boldsymbol{\phi}\right] = \mathbb{P}\left[\bigcap_{j=1}^{M} \left\{R_j \Theta_j(\boldsymbol{\phi}) = \psi_j - \phi_j\right\}\right] \tag{23}$$

where $\cap$ denotes set intersection so $\mathbb{P}[A \cap B]$ is the probability of both A and B occurring. Note that in this form, the ϕ_j and ψ_j symbols are just constants and that the only random variables are the R_j which are independent of one another and thus we may separate the probability as a product

$$\Gamma\left[\boldsymbol{\psi}|\boldsymbol{\phi}\right] = \prod_{j=1}^{M} \mathbb{P}\left[R_j \Theta_j(\boldsymbol{\phi}) = \psi_j - \phi_j\right]. \tag{24}$$

Recall that there is a crushing zone $\mathcal{A}_j^{g^*} \subseteq \mathbb{R}^M$ for each cell j within which crushing will occur and manifests itself within each $\Theta_j(\boldsymbol{\psi}) = \mathbf{1}_{A_j}(\boldsymbol{\psi})$. Meanwhile, it is easy to show that the proposition

$$R_j \Theta_j(\boldsymbol{\phi}) = \psi_j - \phi_j \tag{25}$$

is logically equivalent to

$$\left(R_j = \psi_j - \phi_j \wedge \boldsymbol{\phi} \in \mathcal{A}_j^{g^*}\right) \vee \left(\psi_j = \phi_j \wedge \boldsymbol{\phi} \in \bar{\mathcal{A}}_j^{g^*}\right) \tag{26}$$

where $\wedge$ denotes *and* while $\vee$ denotes *or*. Noting that the two statements in the parentheses are mutually exclusive, we have

$$\mathbb{P}\left[R_j \Theta_j(\boldsymbol{\phi}) = \psi_j - \phi_j\right] = \mathbb{P}\left[R_j = \psi_j - \phi_j \wedge \boldsymbol{\phi} \in \mathcal{A}_j^{g^*}\right] + \mathbb{P}\left[\psi_j = \phi_j \wedge \boldsymbol{\phi} \in \bar{\mathcal{A}}_j^{g^*}\right]$$

$$= f(\psi_j - \phi_j)\mathbf{1}_{\mathcal{A}_j^{g^*}}(\boldsymbol{\phi}) + \delta(\psi_j - \phi_j)\mathbf{1}_{\bar{\mathcal{A}}_j^{g^*}}(\boldsymbol{\phi}), \tag{27}$$

where we have used f as the probability density function of the fragment distribution $\mathcal{F}$ and δ is the Dirac delta function, defined with a probability density

$$\delta(x) := \begin{cases} 0 & \text{if } x \neq 0 \\ \infty & \text{if } x = 0 \end{cases} \tag{28}$$

such that $\int_{-\infty}^{\infty} \delta(x)\, dx = 1$. This finally gives the transition probability as

$$\Gamma\left[\boldsymbol{\psi}|\boldsymbol{\phi}\right] = \prod_{j=1}^{M} \left[f(\psi_j - \phi_j)\mathbf{1}_{\mathcal{A}_j^{g^*}}(\boldsymbol{\phi}) + \delta(\psi_j - \phi_j)\mathbf{1}_{\bar{\mathcal{A}}_j^{g^*}}(\boldsymbol{\phi})\right]. \tag{29}$$

4.3. Time-evolution of the probability density function

To recover the actual state on the next time step given a transition probability, we may use the *law of total probability* which states that the probability for an event A is

$$\mathbb{P}[A] = \sum_n \mathbb{P}[A|B_n]\mathbb{P}[B_n] \tag{30}$$

where $\{B_n\}$ is a set of mutually exclusive events which cover the entire sample space. In our case of continuous variables, we write

$$\mathcal{L}\big[\rho^t(\boldsymbol{\psi})\big] = \rho^{t+1}(\boldsymbol{\psi}) = \int \Gamma\big[\boldsymbol{\psi}|\boldsymbol{\phi}\big]\rho^t(\boldsymbol{\phi})\, d^M\phi \tag{31}$$

where the integral is over all $\mathbb{R}^M$. Using the transition probability in Eq. (29), we see that the time-evolution rule is

$$\rho^{t+1}(\boldsymbol{\psi}) = \int d^M\phi \prod_{j=1}^{M}\Big[f(\psi_j-\phi_j)\mathbf{1}_{\mathcal{A}_j^{g^*}}(\boldsymbol{\phi}) + \delta(\psi_j-\phi_j)\mathbf{1}_{\bar{\mathcal{A}}_j^{g^*}}\boldsymbol{\phi})\Big]\rho^t(\boldsymbol{\phi}). \tag{32}$$

To express this time-evolution rule in a simpler and more intuitive way, for each M-dimensional binary vector $\boldsymbol{\theta} \in \{0,\,1\}^M$ that represents a possible crushing configuration we may define a corresponding set

$$\mathcal{A}_{\boldsymbol{\theta}}^{g^*} := \{\boldsymbol{\psi} \in \mathbb{R}^M \mid \theta_j = \Theta_j(\vec{\psi})\ \forall j = 1,2,\ldots,M\} \tag{33}$$

$$= \{\boldsymbol{\psi} \in \mathbb{R}^M \mid \mathbf{1}_{\mathcal{A}_j^{g^*}}(\boldsymbol{\psi}) = \theta_j\ \forall j = 1,2,\ldots,M\} \tag{34}$$

that represents the region where such a crushing configuration $\boldsymbol{\theta} = (\theta_1,\theta_2,\ldots,\theta_M)$ will occur.

For example, when $M = 2$, the set $\mathcal{A}_{00}^{g^*}$ denotes the zone of no crushing in all cells, $\mathcal{A}_{01}^{g^*}$ denotes the region where cell 1 is not crushing and cell 2 is crushing, $\mathcal{A}_{10}^{g^*}$ denotes the region where cell 1 is crushing and cell 2 is not crushing and $\mathcal{A}_{11}^{g^*}$ denotes the region where both cells 1 and 2 are crushing.

This allows us to write

$$\rho^{t+1}(\boldsymbol{\psi}) = \int d^M\phi\, \rho^t(\boldsymbol{\phi}) \sum_{\boldsymbol{\theta}\in\{0,1\}^M} \mathbf{1}_{\mathcal{A}_{\boldsymbol{\theta}}^{g^*}}(\boldsymbol{\phi}) \prod_{j=1}^{M}\big[f^{\theta_j}(\psi_j-\phi_j)\delta^{1-\theta_j}(\psi_j-\phi_j)\big] \tag{35}$$

since the terms in the product are always either $f(\psi_j-\phi_j)$ if $\theta_j = 1$ or $\delta(\psi_j-\phi_j)$ if otherwise $\theta_j = 0$. This naturally leads us to define a generalised M-dimensional fragment distribution

$$\gamma_{\boldsymbol{\theta}}(\mathbf{r}) := \prod_{j=1}^{M} f^{\theta_j}(r_j)\delta^{1-\theta_j}(r_j) \tag{36}$$

associated with each crushing configuration $\boldsymbol{\theta} \in \{0,\,1\}^M$. For example, in the case $M = 2$, we simply have $\gamma_{00}(r_1,r_2) = \delta(r_1)\delta(r_2)$, $\gamma_{01}(r_1,r_2) = \delta(r_1)f(r_2)$, $\gamma_{10}(r_1,r_2) = f(r_1)\delta(r_2)$ and $\gamma_{11}(r_1,r_2) = f(r_1)f(r_2)$. The time-evolution equation then becomes

$$\rho^{t+1}(\boldsymbol{\psi}) = \sum_{\boldsymbol{\theta}\in\{0,1\}^M} \int d^M\phi\, \rho^t(\boldsymbol{\phi})\mathbf{1}_{\mathcal{A}_{\boldsymbol{\theta}}^{g^*}}(\boldsymbol{\phi})\gamma_{\boldsymbol{\theta}}(\boldsymbol{\psi}-\boldsymbol{\phi}) \tag{37}$$

which is in the form of a convolution equation

$$\rho^{t+1}(\boldsymbol{\psi}) = \sum_{\boldsymbol{\theta}\in\{0,1\}^M} \Big[\Big(\rho^t\mathbf{1}_{\mathcal{A}_{\boldsymbol{\theta}}^{g^*}}\Big) * \gamma_{\boldsymbol{\theta}}\Big](\boldsymbol{\psi}) \tag{38}$$

where we have used the convolution operator $*$ defined between any two scalar functions f and g as $(f*g)(\boldsymbol{\psi}) = \int d^M\phi\, f(\boldsymbol{\phi})g(\boldsymbol{\psi}-\boldsymbol{\phi})$. We may also drop the explicit $\boldsymbol{\psi}$ variables to consider the time-evolution operator $\mathcal{L}$ as a functional that maps distributions to distributions so that

$$\mathcal{L}[\rho] = \sum_{\boldsymbol{\theta}\in\{0,1\}^M} \Big(\rho\mathbf{1}_{\mathcal{A}_{\boldsymbol{\theta}}^{g^*}}\Big) * \gamma_{\boldsymbol{\theta}} = \sum_{\boldsymbol{\theta}\in\{0,1\}^M} \rho * \Big(\gamma_{\boldsymbol{\theta}}\mathbf{1}_{\mathcal{A}_{\boldsymbol{\theta}}^{g^*}}\Big) \tag{39}$$

$$\mathcal{L}[\rho] = \rho * \sum_{\boldsymbol{\theta}\in\{0,1\}^M} \gamma_{\boldsymbol{\theta}}\mathbf{1}_{\mathcal{A}_{\boldsymbol{\theta}}^{g^*}} \tag{40}$$

where we have used the identity $(f\mathbf{1}_{\mathcal{A}}) * g = f * (g\mathbf{1}_{\mathcal{A}})$ and linearity of convolution. Hence time-evolution is merely a convolution

$$\mathcal{L}[\rho] = \rho * \kappa^{g^*} \tag{41}$$

with some *kernel* distribution κ^{g^*}, which for a given stress ratio g^* is

$$\kappa^{g^*} = \sum_{\boldsymbol{\theta}\in\{0,1\}^M} \gamma_{\boldsymbol{\theta}} \mathbf{1}_{\mathcal{A}_{\boldsymbol{\theta}}^{g^*}}. \tag{42}$$

Since the crushing zones $\mathcal{A}_{\boldsymbol{\theta}}^{g^*}$ are disjoint sets, $\kappa^{g^*}(\psi) = \gamma_{\boldsymbol{\theta}}(\psi)$ if and only if $\psi \in \mathcal{A}_{\boldsymbol{\theta}}^{g^*}$ for each configuration $\boldsymbol{\theta} \in \{0, 1\}^M$. Hence the kernel is a function defined piecewise over each crush zone. For example, when $M = 2$, the kernel in piecewise form is

$$\kappa^{g^*}(\boldsymbol{\psi}) = \begin{cases} \delta(\psi_1)\delta(\psi_2) & \text{if } \boldsymbol{\psi} \in \mathcal{A}_{00}^{g^*} \\ \delta(\psi_1)f(\psi_2) & \text{if } \boldsymbol{\psi} \in \mathcal{A}_{01}^{g^*} \\ f(\psi_1)\delta(\psi_2) & \text{if } \boldsymbol{\psi} \in \mathcal{A}_{10}^{g^*} \\ f(\psi_1)f(\psi_2) & \text{if } \boldsymbol{\psi} \in \mathcal{A}_{11}^{g^*}. \end{cases} \tag{43}$$

Note that we name κ^{g^*} the kernel distribution because $\mathcal{L}[\delta] = \delta * \kappa^{g^*} = \kappa^{g^*}$ is the distribution after one time step resulting from a uniform grainsize distribution of only one grainsize, which is analogous to the Green's function of an inhomogeneous differential equation.[1]

This is the incredibly simple form of the operator in the governing time-evolution equation $\rho^{t+1} = \mathcal{L}\left[\rho^t\right]$ and is an exact reformulation of the original stochastic lattice model. If we interpret the probability distributions to actually *be* the state of the system, then we have a deterministic formulation of a statistically equivalent theory.

4.4. Recovery of the empirical distribution

While we have derived the time-evolution of the M-dimensional probability distribution function $\rho(\boldsymbol{\psi})$, a test of its predictive power is to calculate the overall grainsize distribution of the representative volume element, for example by *marginalising*.

Suppose we choose the jth cell and integrate out all the other grainsize variables to obtain the *marginal distribution* $\tilde{\rho}(\psi_j)$ for the jth cell.

$$\tilde{\rho}(\psi_j) = \int d\psi_1\, d\psi_2 \,\ldots\, d\psi_{j-1}\, d\psi_{j+1} \ldots d\psi_M\, \rho(\psi_1, \psi_2, \ldots, \psi_M). \tag{44}$$

As no cell is special, this should be the same for all j and hence we define this unique function $\tilde{\rho}(\psi)$ to be *the* grainsize distribution of the entire representative volume element. Upon performing this operation, all the correlations of the M-dimensional joint distribution function that represent the grainsize fabric of the particles are lost as we map into a one-dimensional distribution function. This operation is thus irreversible.

5. Symmetry-simplified model

If one were to be ignorant of symmetry, the crushing must in general be characterised by M different crushing criteria $g^* \geq g_j(\boldsymbol{\psi})$ for each cell $j \in \{1, 2, \ldots, M\}$, where g_j also depends on all M components of $\boldsymbol{\psi} \in \mathbb{R}^M$. This high-dimensionality is computationally undesirable as the phase space scales exponentially in M. Let us exploit these symmetries of the model to minimise its dimensions.

5.1. Locality

The first symmetry is *locality* – that the time-evolution of the jth cell depends only on a small neighbourhood of nearby cells. This is physically well-motivated since grains only interact with their nearest neighbours. As described thus far, the critical stress g_j at cell j depends only on $\psi_{j-1}, \psi_j, \psi_{j+1}$ with

$$g_j(\boldsymbol{\psi}) = g_j\left(\psi_{j-1}, \psi_j, \psi_{j+1}\right) \tag{45}$$

for each $j = 1, 2, 3, \ldots, M$. This decomposes each M-dimensional function g_j into M three-dimensional functions. This also means that we only need to track M three-dimensional *marginal distributions* $\tilde{\rho}_j(\psi_{j-1}, \psi_j, \psi_{j+1})$ obtained by marginalising out the non-local degrees of freedom.

5.2. Translational invariance

With periodic boundary conditions in j, the second symmetry of the system is *translational invariance* – that any cyclic permutation of the cells will result in the same model. In other words, shifting all the cells by a constant number of cells leaves the system's time-evolution rule unchanged. That is, for any two cells $i, j \in \{1, 2, \ldots, M\}$, their crushing stress ratios

[1] e.g. the deflection due to a point load on a beam is the Green's function of the Euler-Bernoulli beam equation.

$g_i(\psi_{i-1}, \psi_i, \psi_{i+1})$ and $g_j\big(\psi_{j-1}, \psi_j, \psi_{j+1}\big)$ are in fact from the same function $g = g_i = g_j$. In terms of distributions, translational invariance means that regardless of which cell j is chosen, we will still get the same three-dimensional marginal distribution $\tilde{\rho}(\psi_{i-1}, \psi_i, \psi_{i+1}) = \tilde{\rho}\big(\psi_{j-1}, \psi_j, \psi_{j+1}\big) = \tilde{\rho}(\psi_1, \psi_2, \psi_3)$. Thus we only need to keep track of a three-dimensional scalar function.

5.3. Cell reflection symmetry

The third symmetry is that the system is invariant under reversing the order of the cells, as there is no preferred direction in the labelling. This manifests itself as the invariance of the stress function under the reversal of cells with

$$g(\psi_{j-1}, \psi_j, \psi_{j+1}) = g(\psi_{j+1}, \psi_j, \psi_{j-1}). \tag{46}$$

This is important since any such function may be reparameterised in terms of ψ_j and an "average" neighbour grainsize $\bar{\psi}_j = \chi(\psi_{j-1}, \psi_{j+1}) = \chi(\psi_{j+1}, \psi_{j-1})$ for any symmetric function χ such that

$$g\big(\psi_j, \bar{\psi}_j\big) = g\big(\psi_{j-1}, \psi_j, \psi_{j+1}\big). \tag{47}$$

To be consistent with Marks and Einav (2015, 2017) where $\bar{s}_j := \big(s_{j-1} + s_{j+1}\big)/2$, we may enforce $\bar{\psi}_j = \log \bar{s}_j$ so that

$$\bar{\psi}_j = \log\left(\frac{e^{\psi_{j-1}} + e^{\psi_{j+1}}}{2}\right). \tag{48}$$

These symmetries are reflected in the probability density function in that we only need a 2D probability distribution function $\rho^t\big(\psi, \bar{\psi}\big)$ that evolves according to

$$\rho^{t+1}\big(\psi, \bar{\psi}\big) = \mathcal{L}\big[\rho^t\big]\big(\psi, \bar{\psi}\big) \tag{49}$$

for some linear time-evolution operator $\mathcal{L}$.

Note that the system has no time-reversal symmetry since crushing is irreversible.

5.4. Simplified two-dimensional model

With these symmetries in mind, it should be sufficient to represent the state of the system using a 2-dimensional joint distribution function $\rho\big(\psi, \bar{\psi}\big)$ which evolves according to the exact Eq. (40). It is a powerful approximation to use the same time-evolution rule with dimension $M = 2$ that would have the same statistical properties as that of the large model with $M \to \infty$. This is justified since in the slow limit of *event-driven* dynamics, there is only at most one crushing event at each time step and every interaction is a local interaction.

This satisfies our goal of finding a simple and computationally scalable deterministic continuum model for comminution that reproduces the behaviour of the stochastic lattice model.

Let us explicitly write down the symmetry-simplified two-dimensional model. Recall that the functional time-evolution rule is $\rho^{t+1} = \rho^t * \kappa^{g^*}$. By the symmetry arguments made in the previous section, we may take $M = 2$ and rename our grainsize variables as $\psi_1 = \psi$ and $\psi_2 = \bar{\psi}$ to be the parameters of the state function $\rho^t(\psi, \bar{\psi})$. The binary vectors describing the possible crushing states are then $\boldsymbol{\theta} \in \{00, 01, 10, 11\}$. The time-evolution may then be written as

$$\boxed{\rho^{t+1}(\psi, \bar{\psi}) = \int_{-\infty}^{\infty}\int_{-\infty}^{\infty} d\phi\, d\bar{\phi}\, \rho^t(\phi, \bar{\phi})\, \kappa^{g^*}(\phi - \psi, \bar{\phi} - \bar{\psi})} \tag{50}$$

where the kernel distribution κ^{g^*} for a given externally applied stress g^* may be piecewise defined over each crushing zone in terms of generalised fragment distributions by

$$\kappa^{g^*}(\psi, \bar{\psi}) := \begin{cases} \delta(\psi)\delta(\bar{\psi}) & \text{if } (\psi, \bar{\psi}) \in \mathcal{A}_{00}^{g^*} \\ \delta(\psi) f(\bar{\psi}) & \text{if } (\psi, \bar{\psi}) \in \mathcal{A}_{01}^{g^*} \\ f(\psi)\delta(\bar{\psi}) & \text{if } (\psi, \bar{\psi}) \in \mathcal{A}_{10}^{g^*} \\ f(\psi) f(\bar{\psi}) & \text{if } (\psi, \bar{\psi}) \in \mathcal{A}_{11}^{g^*} \end{cases} \tag{51}$$

where f is the fragment distribution with support over $(-\infty, 0]$, δ is the Dirac delta function and the regions are explicitly given by

$$\mathcal{A}_{00}^{g^*} = \{(\psi, \bar{\psi}) \in \mathbb{R}^2 \mid g^* < g(\psi, \bar{\psi}) \text{ and } g^* < g(\bar{\psi}, \psi)\} \tag{52}$$

$$\mathcal{A}_{01}^{g^*} = \{(\psi, \bar{\psi}) \in \mathbb{R}^2 \mid g^* < g(\psi, \bar{\psi}) \text{ and } g^* \geq g(\bar{\psi}, \psi)\} \tag{53}$$

$$\mathcal{A}_{10}^{g^*} = \{(\psi, \bar{\psi}) \in \mathbb{R}^2 \mid g^* \geq g(\psi, \bar{\psi}) \text{ and } g^* < g(\bar{\psi}, \psi)\} \tag{54}$$

$$\mathcal{A}_{11}^{g^*} = \{(\psi, \bar{\psi}) \in \mathbb{R}^2 \mid g^* \geq g(\psi, \bar{\psi}) \text{ and } g^* \geq g(\bar{\psi}, \psi)\}, \tag{55}$$

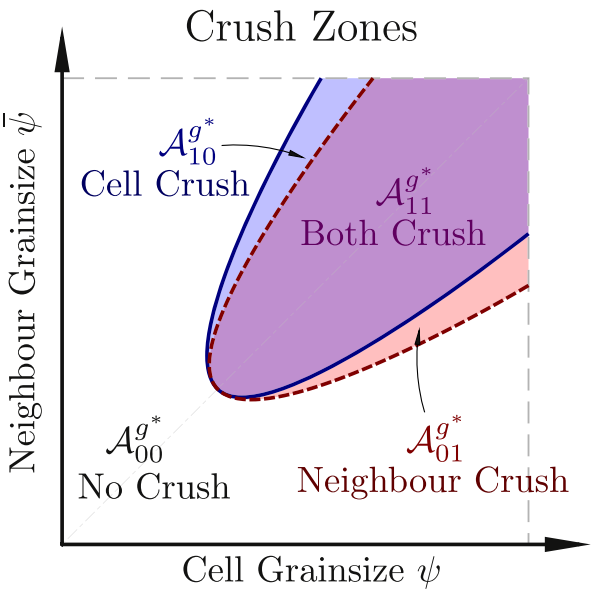

Fig. 4. The crushing zones for the two-dimensional $(\psi, \bar{\psi})$ simplified model where the cell grainsize ψ and neighbour grainsize $\bar{\psi}$ are treated equally. The blue solid line encloses the $\mathcal{A}_{10}^{g^*}$ zone where the ψ cells will crush while the red dashed line encloses the $\mathcal{A}_{01}^{g^*}$ zone where the $\bar{\psi}$ cells will crush. The overlapping zone $\mathcal{A}_{11}^{g^*}$ is the zone where both will crush. As the applied load g^* is increased, these crush zones expand and expel any probability density $\rho(\psi, \bar{\psi})$ into the $\mathcal{A}_{00}^{g^*}$ no crush zone. Note the relative positions of the zones and how they are connected. Under slow crushing the state never enters the $\mathcal{A}_{11}^{g^*}$ zone except along the line $\psi = \bar{\psi}$. (For interpretation of the references to colour in this figure legend, the reader is referred to the web version of this article.)

where the stress function $g(\psi, \bar{\psi})$ takes the form of Eq. (15). A schematic plot of these regions is shown in Fig. 4.

The experimentally observable grainsize distribution $\tilde{\rho}(\psi)$ is obtained by marginalising out the $\bar{\psi}$ with

$$\tilde{\rho}^t(\psi) = \int_{-\infty}^{\infty} d\bar{\psi}\, \rho^t(\psi, \bar{\psi}). \tag{56}$$

Note that in general, the externally applied stress $g^* = g^*(t)$ varies as a function of time and defines the load path of the system. From these equations alone, it is enough to construct efficient numerical algorithms that deterministically reproduce the statistics of the stochastic lattice model.

6. Fast numerical implementation

The simplified model was numerically implemented as a discrete convolution

$$\rho^{t+1}(\psi, \bar{\psi}) = \left(\rho^t * \kappa^{g^*}\right)(\psi, \bar{\psi}). \tag{57}$$

For a given load ratio g^* and fragment distribution $f(\psi)$, the kernel κ^{g^*} is defined piecewise for each region $\mathcal{A}_{00}^{g^*}$, $\mathcal{A}_{01}^{g^*}$, $\mathcal{A}_{10}^{g^*}$ and $\mathcal{A}_{11}^{g^*}$. In numerical implementations, the grainsize ψ may be discretised and truncated into N bins centred at $\psi_1, \psi_2, \ldots, \psi_N$ which range linearly from $\psi_{\min} = \psi_1$ to $\psi_{\max} = \psi_N$. The state ρ^t is then discretised into an $N \times N$ discrete probability mass function with values p_{ij}^t. Meanwhile, the fragment distribution would also be analogously discretised into components $f_j := \int_{\phi_{j-1}}^{\phi_j} d\phi\, f(\phi)$, where the index j runs from 1 to N, although $f_j = 0$ if $\phi_j \geq 0$ to ensure that grainsizes only reduce in size. Similarly the kernel distribution becomes a 2D array K^{g^*} with elements given by

$$K_{i,j}^{g^*} := \int_{\phi_{i-1}}^{\phi_i} \int_{\phi_{j-1}}^{\phi_j} d\phi\, d\bar{\phi}\, \kappa^{g^*}\left(\phi, \bar{\phi}\right). \tag{58}$$

The sets $\mathcal{A}_{00}^{g^*}$, $\mathcal{A}_{01}^{g^*}$, $\mathcal{A}_{10}^{g^*}$ and $\mathcal{A}_{11}^{g^*}$ then become sets of points rather than regions in $\mathbb{R}^2$ and correspondingly the kernel distribution also becomes discretised as

$$K_{i,j}^{g^*} := \begin{cases} \delta_i \delta_j & \text{if } (i,j) \in \mathcal{A}_{00}^{g^*} \\ \delta_i f_j & \text{if } (i,j) \in \mathcal{A}_{01}^{g^*} \\ f_i \delta_j & \text{if } (i,j) \in \mathcal{A}_{10}^{g^*} \\ f_i f_j & \text{if } (i,j) \in \mathcal{A}_{11}^{g^*}. \end{cases} \tag{59}$$

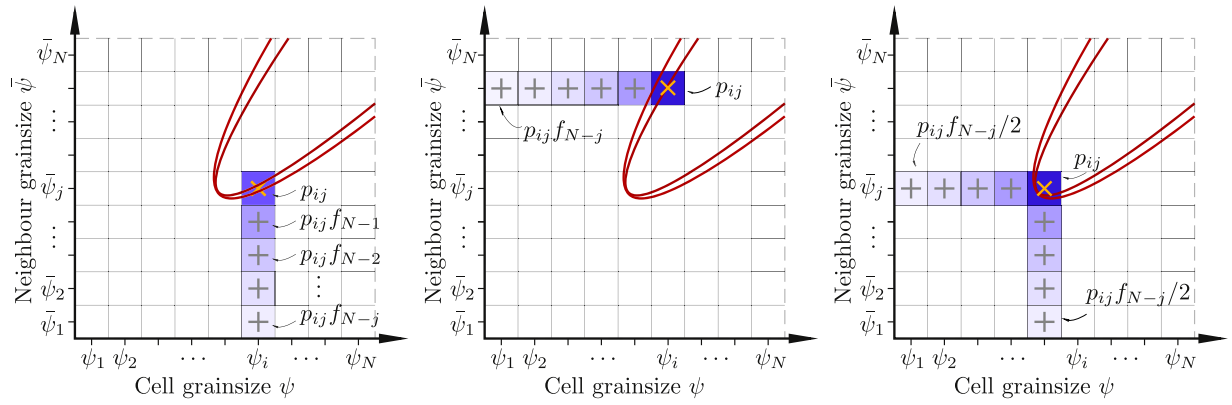

Fig. 5. Visualisation of the two-dimensional fragment distribution kernel $K^{g^*}_{i,j}$ in Eq. (63) as a fragment distribution coming from different (i, j) cells marked with an X shown for crush zones $\mathcal{A}^{g^*}_{01}$, $\mathcal{A}^{g^*}_{10}$ and $\mathcal{A}^{g^*}_{11}$ respectively (left to right). The probability $p_{i,j}$ at cell (i, j) becomes zero at the next time step and is distributed according to this two-dimensional fragment distribution as shown depending on which zone it is in.

where the Dirac delta functions become discretised as

$$\delta_j = \begin{cases} 1 & \text{if } j = 0 \\ 0 & \text{if } j \neq 0. \end{cases} \tag{60}$$

The time-evolution rule thus also becomes a discrete convolution

$$\boxed{p^{t+1}_{i,j} = \sum_{k=1}^{N}\sum_{l=1}^{N} p^t_{k,l} K^{g^*}_{k-i,l-j}.} \tag{61}$$

To recover the marginal distribution for $\rho_\Psi(\psi)$, one simply sums over the j indices representing the $\bar{\psi}$ variables to get

$$p^t_i := \sum_{j=1}^{N} p^t_{i,j}, \tag{62}$$

which is the binned form of the experimentally observable grainsize distribution $\tilde{\rho}(\psi)$.

6.1. Simulation details

The cutoffs for the range of grainsizes ψ to consider were arbitrarily chosen at $\psi_{\min} = -6$ and $\psi_{\max} = 1$, such that the grainsize may vary over three orders of magnitude. Of course, the model can be simulated over an even greater range at a cost of either speed or resolution.

If the crushing is sufficiently slow, we may make the smoothing approximation that the generalised fragment distribution is

$$K^{g^*}_{i,j} := \begin{cases} \delta_i\delta_j & \text{if } (i,j) \in \mathcal{A}^{g^*}_{00} \\ \delta_i f_j & \text{if } (i,j) \in \bar{\mathcal{A}}^{g^*}_{00} \text{ and } i > j \\ f_i\delta_j & \text{if } (i,j) \in \bar{\mathcal{A}}^{g^*}_{00} \text{ and } i < j \\ \big(\delta_i f_j + f_i\delta_j\big)/2 & \text{if } (i,j) \in \bar{\mathcal{A}}^{g^*}_{00} \text{ and } i = j. \end{cases} \tag{63}$$

The mathematical motivation behind this approximation is that when the crushing zones advance slowly from the unloaded state, every point in $\mathbb{R}^2$ starts off in the non-crushing zone $\mathcal{A}^{g^*}_{00}$ as shown in Fig. 4. As the load g^* is increased, the crushing zone slowly expands but the point must at some point be inside one of the single-cell crushing regions $\mathcal{A}^{g^*}_{01}$ or $\mathcal{A}^{g^*}_{10}$ rather than the two-cell crushing zone $\mathcal{A}^{g^*}_{11}$. The only exception is the unlikely case $\psi = \bar{\psi}$, which is usually an artefact of coarse binning, in which case it is sensible to take the "average" fragment distribution in the last case when $i = j$. This is visualised in Fig. 5 for each of the non-trivial cases.

The physical justification is that under slow crushing, cells may only crush one at a time so the only crushing configurations allowed are 00 which is no crushing, 01 which is the second cell crushing only and 10 which is the first cell crushing only. The crushing state 11 is forbidden under slow crushing as two adjacent cells are not allowed to crush at the same time as one must crush before the other.

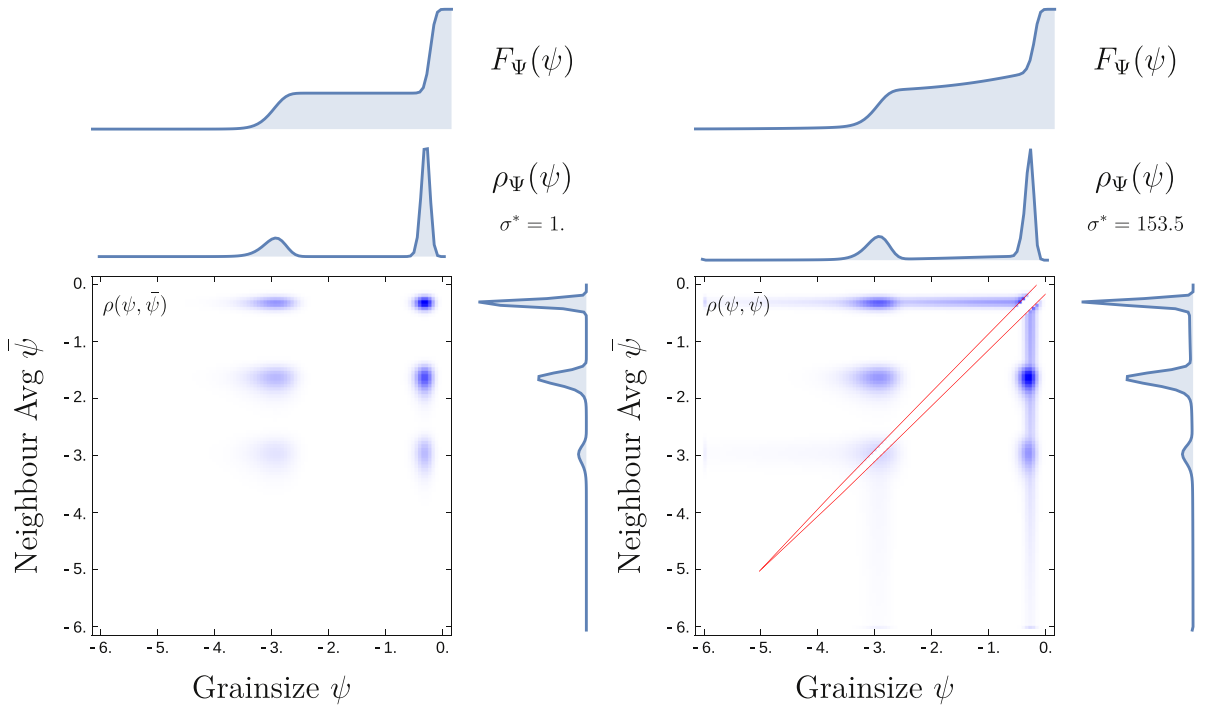

Fig. 6. Density plot of the joint probability density function and its associated marginal distributions $\tilde{\rho}(\psi)$ above it and the overall grainsize distribution as a CDF for a bivariate distribution. The left plots are the initial distribution and the right plot is time-evolved by slow crushing. The red curves denote the extent of the crushing zones. (For interpretation of the references to colour in this figure legend, the reader is referred to the web version of this article.)

6.2. Mixing

When initialising the cells, it is useful to be able to model complete mixing when the Ψ and $\bar{\Psi}$ random variables become completely independent of one another while still retaining the same overall distribution $\tilde{\rho}(\psi)$. When this is the case, the distribution function is *separable* into a product distribution

$$\rho\left(\psi, \bar{\psi}\right) = \rho_\Psi(\psi)\rho_{\bar{\Psi}}(\bar{\psi}), \tag{64}$$

where ρ_Ψ and $\rho_{\bar{\Psi}}$ are marginal probability distributions for Ψ and $\bar{\Psi}$ respectively. This independence is lost when crushing occurs and the two variables Ψ and $\bar{\Psi}$ become correlated in a complex way described by the joint distribution. This encodes the *grainsize fabric* or arrangement of the grains.

Note that these two distributions are not identical even in the independent case. However, when they are independent, they are related by a transformation based on the form of the averaging function. When one uses the geometric mean on s, which is the arithmetic mean on ψ with

$$\bar{\Psi}_j := \frac{\Psi_{j-1} + \Psi_{j+1}}{2}, \tag{65}$$

the distribution for $\bar{\Psi}$ is simply

$$\rho_{\bar{\Psi}}(\bar{\psi}) = \int d\psi \, 2\rho_\Psi(\psi)\rho_\Psi(2\bar{\psi} - \psi). \tag{66}$$

When the relationship is more complicated, for instance in our canonical choice of $\bar{\Psi} = \log S$ in Eq. (48), the transformed distribution may in general be computed from the cumulative probability distribution from first principles. This is shown in Fig. 6 for an example of initially gap-graded distribution and a time-evolved distribution.

7. Numerical simulations and results

We have in the above sections resolved the homogenised evolution Eq. (50) that analytically describes the smooth limit of the stochastic lattice model, as well as described its fast numerical deterministic implementation through Eq. (61). Here, results from this newly resolved continuum model are evaluated against the equivalent stochastic lattice model simulations. To demonstrate the success of the new formulation, in this section we illustrate that the newly established continuum model effectively captures the same grainsize dynamics as in the stochastic lattice model for entirely different initial distributions.

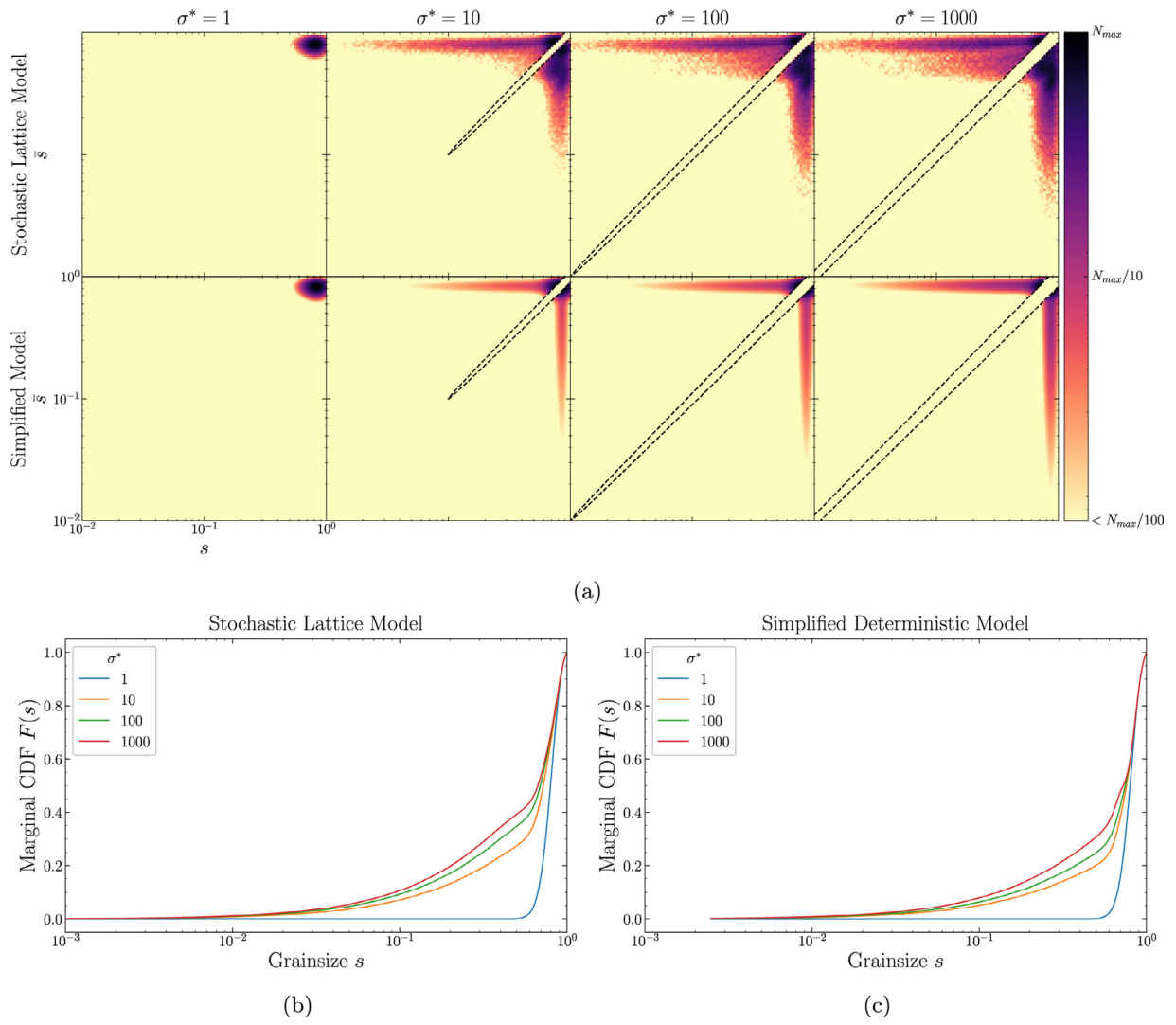

Fig. 7. Crushing from a uniformly graded initial grainsize distribution modelled using the stochastic lattice model and the simplified model. (a) Comparison of the state evolution the stochastic lattice model (top) and the simplified continuum model (bottom) using the same parameters for a uniformly-graded initial grainsize distribution. (b) CDF of the grainsize distribution evolving under increasing applied stress ratio σ^* for the stochastic lattice model. (c) CDF of the grainsize distribution evolving under increasing applied stress ratio σ^* for the simplified deterministic model.

Since the ability of the stochastic lattice model to capture the right comminution dynamics in closed experimental systems has already been shown (Guida et al., 2020), the comparison below essentially illustrates the power of the newly established continuum comminution model.

Specifically, simulations were performed using the fast numerical deterministic implementation for a variety of different grainsize distributions using the same parameters as those for the stochastic lattice model in Marks and Einav (2017). The time-evolution of the grainsize distributions was then compared against that of the stochastic lattice model. Note that although the evolution rules of the deterministic model are symmetric, here we start off the simulations with a non-symmetric initial two-dimensional joint distribution over (s_1, s_2) to match the initial distribution of the stochastic lattice model model over $(s, \bar{s})$. Given an initial grainsize distribution $\rho_S^0(s)$, this non-symmetric initial state can be taken as $\rho^0(s_1, s_2) = \rho_S^0(s_1)\rho_S^0(s_2)$ with $\rho_S^0(s_2) = \int_0^1 ds\, 2\rho_S^0(s)\rho_S^0(2s_2 - s)$ as the distribution of the neighbour-average grainsize $\bar{S} = (S_- + S_+)/2$ which is an average of two independent random variables S_- and S_+ identically distributed as $\rho_S^0(s)$, which is similar to (66). The physical interpretation for the independence of these variables as an initial condition means that the material starts off as a fabric of grains that are completely mixed with uncorrelated neighbours.

We start by evaluating the model's ability to capture the evolution of the grainsize distribution under uniaxial compression of initially uniformly graded medium (that is, an initially monodisperse granular sample). As shown on Fig. 7

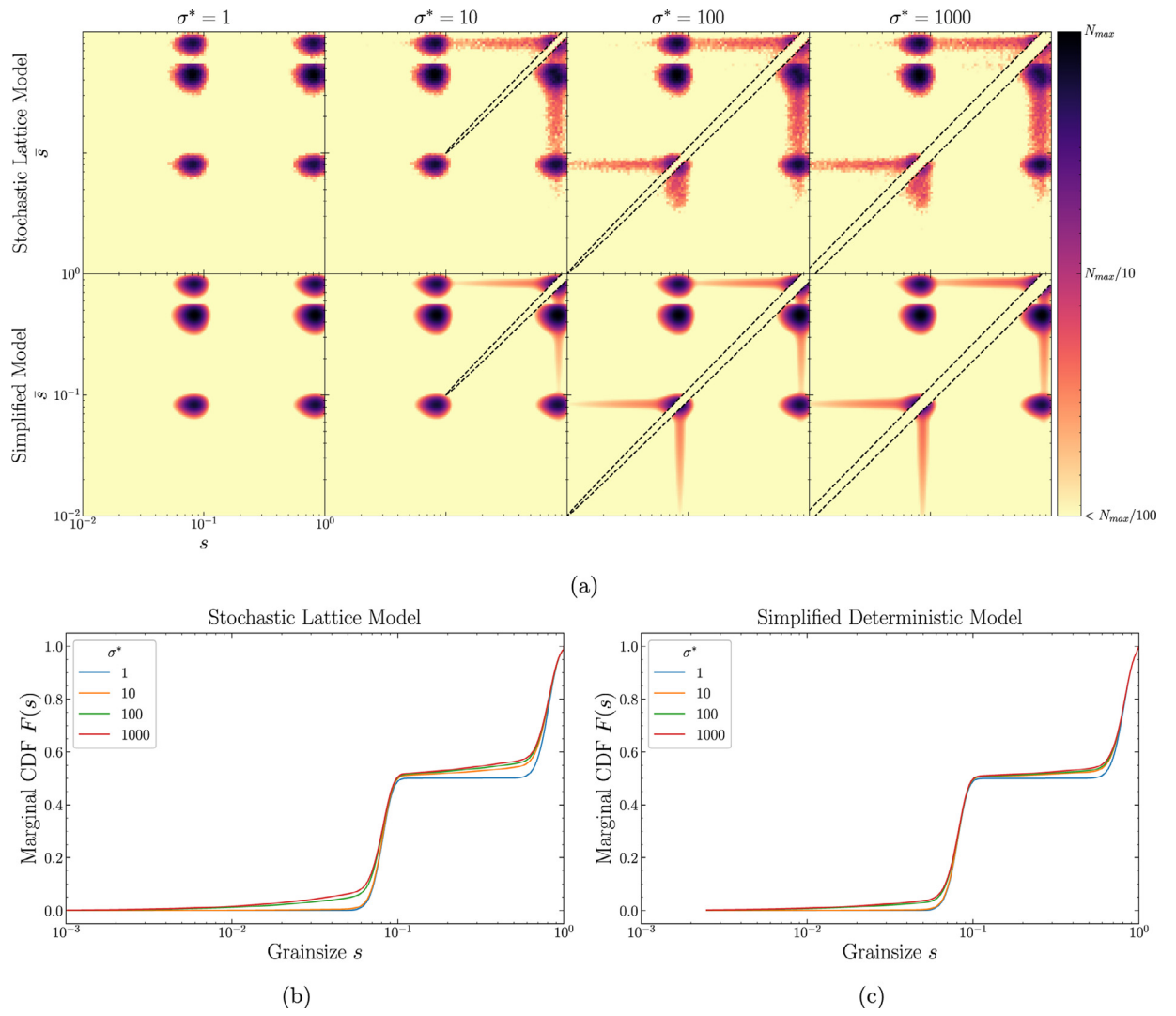

Fig. 8. Crushing from a gap-graded initial grainsize distribution modelled using the stochastic lattice model and the simplified model. (a) Comparison of the state evolution the stochastic lattice model (top) and the simplified continuum model (bottom) using the same parameters for a bivariate gap-graded initial grainsize distribution. (b) CDF of the grainsize distribution evolving under increasing applied stress ratio σ^* for the stochastic lattice model. (c) CDF of the grainsize distribution evolving under increasing applied stress ratio σ^* for the simplified deterministic model.

the model predicts the same dynamics that the stochastic lattice model predicts, both in terms of the progression of the two-dimensional joint distribution over grainsize and local-average grainsize in Fig. 7a and the experimentally measurable marginal grainsize distribution in Fig. 7b. In particular, Fig. 7b reveals the same sort of evolution that many previous experimental studies revealed in the past, as described in Guida et al. (2020). We also note the small qualitative differences in the way fragments are generated in Fig. 7a, where unlike the deterministic continuum model, in the stochastic model they do not purely flow downwards or leftwards. This is because the stochastic model is slightly influenced by infrequent small localised crushing avalanches during individual event-driven computational steps, where the crushing of one cell may trigger immediate crushing of neighbouring cells.

As the second challenge, the initial grainsize distribution is taken to be gap-graded (meaning, an assembly containing only two distinct grainsizes). For example, the size ratio between the large and small particles is here taken to be 10, and each species initially contributes 50% to the overall volume. Similar crushing tests were carried out experimentally by Zhang and Baudet (2014). As shown on Fig. 8, again our newly established continuum model predicts almost identical dynamics that the previously validated stochastic lattice model described, both in terms of the two-dimensional joint distribution on Fig. 8a and the marginal grainsize distribution on Fig. 8b, the latter consistent with the experimental data of Zhang and Baudet (2014). Again, the minor differences in Fig. 8a are due to localised crushing avalanches in the stochastic model.

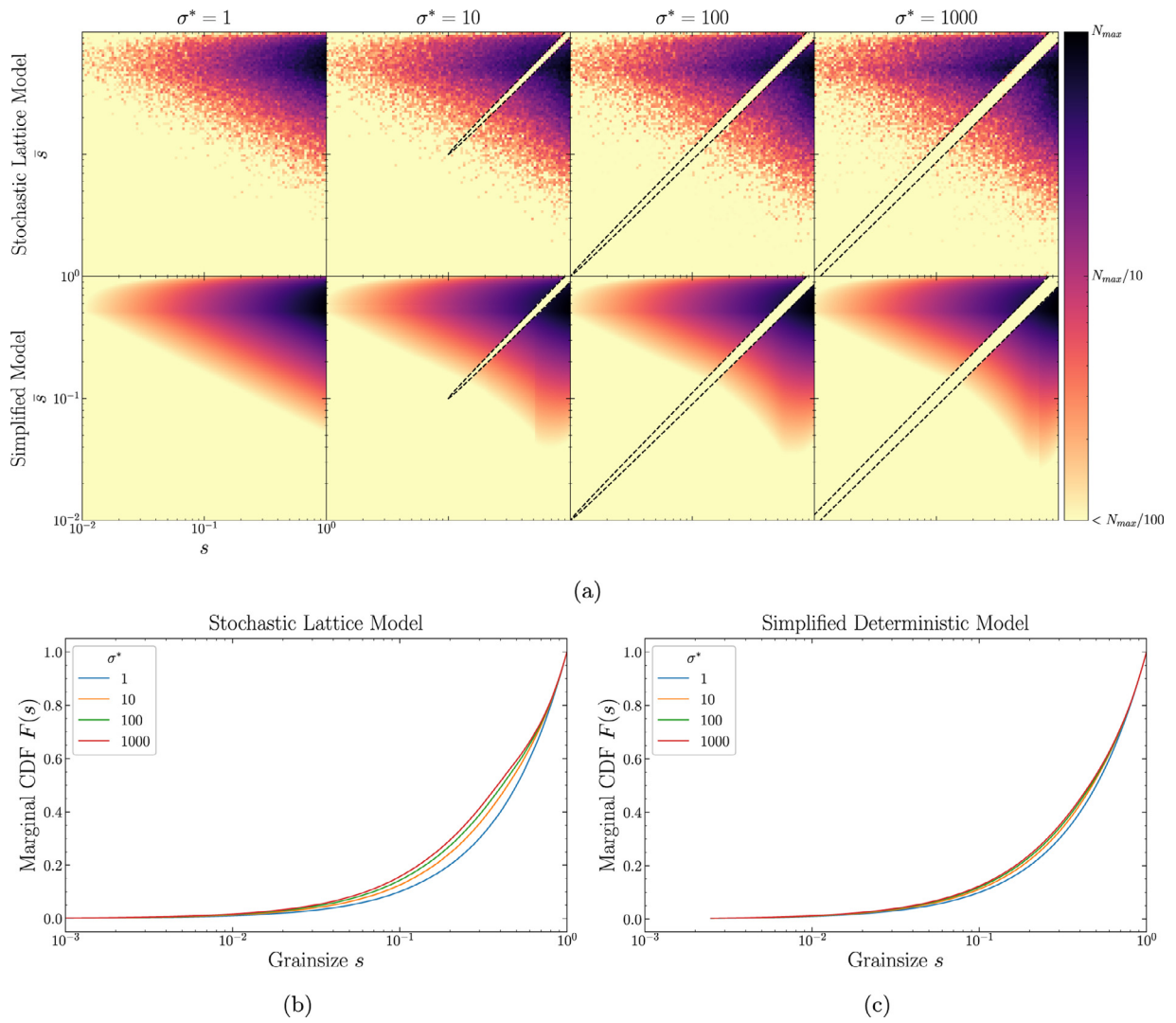

Fig. 9. Crushing from a well-graded initial grainsize distribution modelled using the stochastic lattice model and the simplified model. (a) Comparison of the state evolution the stochastic lattice model (top) and the simplified continuum model (bottom) using the same parameters for a well-graded initial grainsize distribution. (b) CDF of the grainsize distribution evolving under increasing applied stress ratio σ^* for the stochastic lattice model. (c) CDF of the grainsize distribution evolving under increasing applied stress ratio σ^* for the simplified deterministic model.

As the third and final example, we study the grainsize dynamics of an initially well-graded sample (meaning, an initially highly polydisperse medium with many different grainsizes varying over several orders of grainsize magnitudes). As Fig. 9 illustrates, again our newly established continuum model predicts the same dynamics as the previously validated stochastic lattice model predicts, both in terms of the two-dimensional joint distribution seen in Fig. 9a and the marginal grainsize distribution in Fig. 9b. For such cases with initially highly polydisperse media, the grainsize distribution evolves only in a limited way compared with the other two cases above.

Upon qualitative inspection of these plots, it is easy to see that the model well-reproduces the behaviour of the stochastic lattice model. The discrepancies may have arisen from truncation errors with the stochastic lattice model simulation, which was run at a finite discretisation of grainsize and finite time step such that not all crushing events were exactly isolated from adjacent neighbours crushing at the same time step. As such, the newly established continuum comminution model can in fact be regarded as the continuous analog of the experimentally validated stochastic lattice model.

8. Discussion

Below we discuss a few additional aspects related to the newly derived continuum comminution model.

8.1. Extensions to include rate effects

When in situations where the modelling of fast loading is desired, these effects may be considered by a simple superposition of the slow crushing kernel with the fast crushing kernel.

$$K_{i,j}^{g^*} = (1-\alpha)K_{i,j}^{g^*,\text{slow}} + \alpha K_{i,j}^{g^*,\text{fast}} \tag{67}$$

where $\alpha \in [0, 1]$ is a dimensionless parameter that describes the rate of loading. The case $\alpha = 0$ is that of slow loading and $\alpha = 1$ is that of extremely fast-loading. The fast-loading kernel is simply the independent fragment distribution

$$K_{i,j}^{g^*} := \begin{cases} \delta_i \delta_j & \text{if } (i,j) \in \mathcal{A}_{00}^{g^*} \\ f_i f_j & \text{if } (i,j) \in \mathcal{A}_{00}^{g^*}. \end{cases} \tag{68}$$

If the crushing is done infinitesimally slowly each crushing event should happen one at a time. Slow crushing causes the probability distribution function to be correlated since the kernel is not separable unlike that of fast or mixed crushing which may be separated into $\rho(\psi, \bar{\psi}) = \rho_\Psi(\psi)\rho_{\bar{\Psi}}(\bar{\psi})$.

8.2. Computational time and complexity

In general, the time complexity of the convolution algorithm is $O(N^4)$ by inspection of the discrete convolution Eq. (61) for $N \times N$ grainsize bins.

For the case of slow loading however, since the crushing zone advances very slowly, each time step will only have a very small number of new cells in the crushing zone, which for a correctly chosen time step will be restricted to near the boundary. The area of the crush zone is of order $O(N^2)$, while the number of bins on the edge of the boundary is of order $O(N)$. The convolution only needs to be done on these cells, which takes $O(N^2)$ time. This leads to a time-complexity of $O(N^3)$ for each time step. The space complexity is of course just $O(N^2)$ for both cases since it requires the storage of $N \times N$ arrays.

8.3. Generalisation to open system

When the original stochastic lattice model was introduced, it was hoped that segregation, mixing and comminution may all be incorporated into a single differential equation that describes the system. While mixing and segregation were well-described analytically with partial differential equations, this was not possible with comminution.

Since we now know that the rule for comminution is a convolution equation linear in some probability density function, we may apply similar techniques to those for solving linear partial differential equations. In fact, the system in continuous time may be equivalently formulated as non-local partial differential equations, an active area of mathematical research (Bucur and Valdinoci, 2016).

Nevertheless, the clarity of the simplified model and its favourable scaling with low memory requirements should allow it to be scalable into a larger volume of space and time.

As such, representing the system would require a function $\rho(x, y, z, \psi, \bar{\psi})$. This is not inconceivable as the $\rho(\psi, \bar{\psi})$ at each volume element may be binned as an $N \times N$ array and so still scales *linearly* in the volume to be simulated. To generalise the model to three spatial dimensions, one possible approach would be to rephrase the breakage criterion $g \leq g^*$ in terms of stress tensor invariants. Using principles of fracture mechanics, the Weibull stress constant embedded in the crushing function g can be expressed using the particle crushing energy, as derived in Zhang et al. (2016). On the other hand, the scalar stress function g^* can be replaced by stress invariants to calculate the energy available for breakage as motivated by the breakage mechanics theory (Einav, 2007a; 2007b). Other improvements may seek to include the effects of kinetic stress for gaseous-fluid dynamic regimes, an idea that requires future examination. Finally, the derivation of a combined model to include segregation and mixing will also be the natural extension of this work.

9. Conclusion

In conclusion, we have mobilised mathematical tools and arguments to derive a continuum model for comminution that reproduces the behaviour of a physically based stochastic lattice model. While the macroscopic equations of fluid mechanics can be derived by coarse-graining the microscopic equations of classical mechanics, and while the same equations may also be derived by coarse-graining *lattice models* (Shi and Sader, 1998), this paper has demonstrated that the grainsize dynamics of brittle granular media may also be understood by coarse-graining stochastic lattice models.

We achieved this by redefining the original stochastic lattice model of comminution as a stochastic process in M-dimensional Euclidean space and deriving the time-evolution rule for its probability distribution function to give a simple convolution operation with a kernel that is a generalised fragment distribution. Exploiting the symmetries of the stochastic lattice model in its crushing zone geometry that manifests its crushing criterion, we have derived a two-dimensional time-evolution equation that defines a deterministic and grainsize-continuous model.

While a small set of fields in space and time such as stress, density, elastic strain and bulk velocity can statistically capture the macroscopic state of a solid or fluid continuum, no finite set of parameters may sufficiently describe the grainsize if one wishes to describe the distribution $F(s)$ of grainsizes s that is varying continuously in space and time. Naïvely, adding an extra dimension may seem to solve the problem but this is complicated by the fact that macroscopic behaviour is highly sensitive to the microscopic arrangement of the constituent grains (that we termed the grainsize fabric in this paper).

The ultimate model should be generalisable to describe *open comminution* processes that are coupled with the partial differential equations for segregation and mixing (Marks and Einav, 2015; 2017). Mathematically describing the evolution of a representative volume of crushable granular media containing a statistically significant number of grains at the level of grainsize distributions under varying stress conditions is the subject of this paper and a step towards such a model.

Declaration of Competing Interest

The authors declare that they have no known competing financial interests or personal relationships that could have appeared to influence the work reported in this paper.

CRediT authorship contribution statement

Eric Huang: Methodology, Software, Validation, Formal analysis, Investigation, Data curation, Writing - original draft, Visualization. **Benjy Marks:** Conceptualization, Methodology, Data curation, Writing - review & editing, Supervision. **Itai Einav:** Conceptualization, Methodology, Writing - review & editing, Supervision, Project administration.

Acknowledgments

Fruitful discussion with Prof. Ken Kamrin on alternative schemes for homogenising stochastic comminution is greatly acknowledged. Many thanks also to the Australian Research Council for support through projects DP160104310 and DP190103487.

Appendix A. Notation

Table A.1 documents the list of symbols used in this paper. All physical quantities have been normalised to be non-dimensional.

Table A1
List of Symbols.

Symbol	Name	Description
$\mathbf{1}_{\mathcal{A}}$	Indicator function	Function that returns 1 if argument is in $\mathcal{A}$ and 0 otherwise
$\mathcal{A}$	Set	A set of points in some space
$\mathcal{A}_\theta^{\sigma^*}$	Crush zone θ	Set of grainsize states which will crush under applied stress ratio σ^*
$\mathcal{A}_\theta^{g^*}$	Crush zone θ	Set of grainsize states which will crush under logspace applied stress ratio g^*
$f(r)$	PDF for logspace fragment distribution	Probability density function for the logspace grainsize reduction random variable R
f_i	Discretised logspace PMF	Components of probability mass function for fragment distribution
$F(x)$	Cumulative distribution function	Monotonic function from 0 to 1 that defines a probability distribution
$\mathcal{F}$	Logspace fragment distribution	Probability distribution for logspace grainsize reduction factor random variables R_j^t
$\mathcal{F}_X$	Fragment distribution	Probability distribution for grainsize reduction factor random variables X_j^t
g	Logspace stress function	Logspace stress function
g^*	Logspace applied stress ratio	Applied stress in logspace
i	Discretisation index	Integer index for enumeration of continuum discretisation
j	Cell index	Integer index for enumeration of stochastic lattice model cells
k	Rescaling constant	Constant for logspace crushing criterion
$K_{i,j}^{g^*}$	Logspace crushing kernel	Kernel function for convolution
$K_{i,j}^{g^*,\text{slow}}$	Slow logspace crushing kernel	Slow crushing kernel
$K_{i,j}^{g^*,\text{fast}}$	Fast logspace crushing kernel	Fast crushing kernel
L	Time-evolution vector operator	Discrete-time operator that maps logspace grainsize vector state to new logspace grainsize vector state for the next time step
$\mathcal{L}$	Time-evolution functional operator	Discrete-time operator that maps logspace grainsize probability density function to new logspace grainsize probability density function for the next time step
$\boldsymbol{s}$	Grainsize state	Array of grainsizes for each cell

(*continued on next page*)

Table A1 (*continued*)

Symbol	Name	Description
M	Model size	Number of stochastic lattice model cells
n	Scaling parameter	For the stochastic lattice model crushing criterion
N	New grid size	Grid size of the new model discretisation
$\mathbb{N}$	Natural numbers	The set of natural numbers $\{0, 1, 2, \ldots\}$
O	Big-O notation	Asymptotic notation for algorithms
$\mathbb{P}[A]$	Probability	Probability of some event A
$p^t_{i,j}$	Discretised probability mass	Probability mass function terms.
R	Logspace grainsize reduction	Random variable $R = \log X$ with support $-\infty < R \leq 0$
R^t_j	Logspace grainsize reduction	Random variable $R^t_j = \log X^t_j$
$\mathbb{R}$	Real numbers	The set of real numbers
$\mathbb{R}^M$	Euclidean space	M-dimensional Euclidean space
r	Logspace grainsize reduction value	Value of logspace grainsize reduction $r \leq 0$
s	Grainsize	Grainsize value for a model cell $0 < s \leq s_{\max}$
s^t_j	Cell grainsize	Grainsize of cell j at time t
S	Grainsize random variable	Random variable for a cell grainsize
S^t_j	Cell grainsize random variable	Random variable for grainsize of cell j at time t
$\boldsymbol{S}^t$	Grainsize state at time t	Random variable for array of grainsizes at time t
$\bar{s}$	Neighbourhood grainsize	Average of neighbouring cell grainsizes
$\bar{s}^t_j$	Neighbourhood grainsize	Average of neighbouring cell grainsizes around cell j at time t
$s_{\max}$	Maximum grainsize	Reference maximum grainsize
t	Time	Integer time step index
w	Crushing criterion parameter	Weibull parameter for the stochastic lattice model crushing criterion
x	Grainsize reduction factor	Value $0 < x \leq 1$ by which grainsize of a cell reduces after a crushing event
X	Grainsize reduction factor	Random variable $0 < X \leq 1$ that is the factor by which the grainsize of a cell reduces in a crushing event
X^t_j	Grainsize reduction factor	Random variable for grainsize reduction factor in cell j at time t
$\gamma_{\boldsymbol{\theta}}(\boldsymbol{r})$	M-dimensional fragment distribution	Generalized fragment distribution for many cells
$\delta(x)$	Dirac delta function	The unit impulse
δ_{ij}	Kronecker delta function	1 if $i = j$, 0 otherwise
θ	Binary vector	A binary-valued vector for labelling crush zones
Θ	Binary function	Maps from grainsize vector states to 0 if not crushing or 1 if crushing
κ^{g^*}	Crushing kernel	For simplified model
κ	Fragment distribution shape parameter	Shape parameter for Weibull fragment distribution
λ	Fragment distribution scale parameter	Scale parameter for Weibull fragment distribution
$\rho(\psi, \bar{\psi})$	Model PDF state	Probability density function over grainsize and neighbourhood average grainsize that serves as the state in the new model
ρ_X	Fragment PDF	Fragment distribution probability density function $\rho_X(x)$
ρ^t_Ψ	PDF of logspace grainsize state	Probability density function of logspace grainsize configuration at time t
$\tilde{\rho}(\psi)$	Marginal distribution	The probability density function marginalised over other variables
σ	Stress function	Stress function proxy for maximum tensile stress experienced by any grain
σ^*	Applied stress ratio	Ratio of applied stress to stress required for first crushing
ϕ	Dummy logspace grainsize	Dummy logspace grainsize used for derivations
ψ	Logspace grainsize	Logspace grainsize $\psi = \log s$
ψ^t_j	Logspace grainsize	Logspace grainsize of cell j at time t
$\boldsymbol{\psi}$	Logspace grainsize state	Array of logspace grainsize values that defines a state in the stochastic lattice model
Ψ	Logspace grainsize random variable	Random variable for logspace grainsize
Ψ^t_j	Logspace grainsize random variable	Random variable for logspace grainsize in cell j at time t
$\bar{\psi}$	Logspace neighbourhood grainsize	Average logspace grainsize of neighbouring cells
$\boldsymbol{\Psi}^t$	Logspace grainsize random vector	Array of random variables for logspace grainsize in cells at time t
$\sim$	Distributed according to	$X \sim \mathcal{F}_X$ means random variable X is distributed according to probability distribution $\mathcal{F}_X$.
$\wedge$	And	Logical AND operator
$\mathbb{P}[A\|B]$	Conditional probability	Probability of event A given event B
$*$	Convolution	Convolution operator
$:=$	Define	$x := y$ means x is defined as y
$\forall$	For all	Logic operator
$\in$	In	Set inclusion, e.g. $a \in \mathcal{A}$ means element a is in set $\mathcal{A}$.
$\odot$	Hadamard product	Element-wise product of vectors
log	Natural logarithm	Logarithm with base e
$\notin$	Not in	Negation of $\in$
$\vee$	Or	Logical OR operator
$\{.\}$	Set	Set of elements
$\setminus$	Set minus	$\mathcal{A} \setminus \mathcal{B} := \{x \in \mathcal{A} \mid x \notin \mathcal{B}\}$
$(v_1, v_2, \ldots, v_N)$	Vector or array	Ordered set of elements

References

An, L.-J., Sammis, C.G., 1994. Particle size distribution of cataclastic fault materials from southern california: a 3-D study. PAGEOPH 143 (1).

Aranson, I.S., Tsimring, L.S., 2006. Patterns and collective behavior in granular media: theoretical concepts. Rev. Mod. Phys. 78 (2), 641–692. doi:10.1103/RevModPhys.78.641. arxiv: 0507419.

Barndorff-Nielsen, O., 1977. Exponentially decreasing distributions for the logarithm of particle size. Proc. R. Soc. A Math. Phys. Eng. Sci. 353 (1674), 401–419. doi:10.1098/rspa.1977.0041.

Bucur, C., Valdinoci, E., 2016. Nonlocal Diffusion and Applications, 1st Springer doi:10.1007/978-3-319-28739-3. arxiv: 1504.08292.

Castiglione, P., Falcioni, M., Lesne, A., Vulpiani, A., 2008. Chaos and Coarse Graining in Statistical Mechanics. Cambridge University Press, New York, NY, USA.

Dacey, M.F., Krumbein, W.C., 1979. Models of breakage and selection for particle size distributions. J. Int. Assoc. Math. Geol. 11 (2), 193–222. doi:10.1007/BF01028965.

Einav, I., 2007a. Breakage mechanics-Part I: theory. J. Mech. Phys. Solids 55 (6), 1274–1297. doi:10.1016/j.jmps.2006.11.003.

Einav, I., 2007b. Breakage mechanics-Part II: modelling granular materials. J. Mech. Phys. Solids 55 (6), 1298–1320. doi:10.1016/j.jmps.2006.11.004.

Epstein, B., 1947. The mathematical description of certain breakage mechanisms leading to the logarithmico-normal distribution. J. Frankl. Inst. 244 (6), 471–477. doi:10.1016/0016-0032(47)90465-1.

Espanol, P., 2004. Statistical mechanics of coarse-graining. In: Novel Methods in Soft Matter Simulations, pp. 69–115. doi:10.1016/j.cell.2013.07.024. arXiv: 1309.2453v1.

Gay, S.L., 2004. A liberation model for comminution based on probability theory. Miner. Eng. 17 (4), 525–534. doi:10.1016/j.mineng.2003.11.012.

Gilvarry, J.J., 1961. Fracture of brittle solids. i. distribution for fragment size in single fracture (theoretical). J. Appl. Phys. 32 (1961), 391. doi:10.1063/1.1736016.

Göncü, F., Durán, O., Luding, S., 2010. Constitutive relations for the isotropic deformation of frictionless packings of polydisperse spheres. Comptes Rendus Mécanique 338 (10–11), 570–586.

Grady, D.E., Kipp, M.E., 1985. Geometric statistics and dynamic fragmentation. J. Appl. Phys. 58 (3), 1210–1222. doi:10.1063/1.336139. arXiv: 1011.1669v3.

Griffith, A.A., 1921. The phenomena of rupture and flow in solids. Philos. Trans. R. Soc. Lond. Ser. A Contain. Pap. Math. Phys. Character 221, 163–198.

Guida, G., Einav, I., Marks, B., Casini, F., 2020. Linking micro grainsize polydispersity to macro porosity. Int. J. Solids Struct. 187, 75–84.

Halmos, P.R., 1944. Random alms. Ann. Math. Stat. 15 (2), 182–189. doi:10.1214/aoms/1177728422.

Hattori, I., Yamamoto, H., 1999. Rock fragmentation and particle size in crushed zones by faulting. J. Geol. 107 (2), 209–222. doi:10.1086/314343.

King, R., Schneider, C., 1998. Mineral liberation and the batch communition equation. Miner. Eng. 11 (12), 1143–1160. doi:10.1016/S0892-6875(98)00102-2.

Kolmogorov, A.N., 1941. On the logarithmical normal particle size distribution caused by particle crushing. Dokl. Akad. Nauk SSSR 31, 99–101.

Kruyt, N.P., 2012. Micromechanical study of fabric evolution in quasi-static deformation of granular materials. Mech. Mater. 44, 120–129.

Lrincz, J., Imre, E., Gálos, M., Trang, Q.P., Rajkai, K., Fityus, S., Telekes, G., 2005. Grading entropy variation due to soil crushing. Int. J. Geomech. 5 (4), 311–319. doi:10.1061/(ASCE)1532-3641(2005)5:4(311).

Marks, B., Einav, I., 2015. A mixture of crushing and segregation: the complexity of grainsize in natural granular flows. Geophys. Res. Lett. 42 (2), 274–281. doi:10.1002/2014GL062470.

Marks, B., Einav, I., 2017. A heterarchical multiscale model for granular materials with evolving grainsize distribution. Granul. Matter. 19 (3), 61.

Marone, C., Scholz, C.H., 1989. Particle-size distribution and microstructures within simulated fault gouge. J. Struct. Geol. 11 (7), 799–814. doi:10.1016/0191-8141(89)90099-0.

McDowell, G.R., Bolton, M.D., Robertson, D., 1996. The fractal crushing of granular materials. J. Mech. Phys. Solids 44 (12), 2079–2102.

McDowell, G.R., Harireche, O., 2002. Discrete element modelling of soil particle fracture. Géotechnique 52 (2), 131–135. doi:10.1680/geot.2002.52.2.131.

Miao, G., Alonso-Marroquin, F., Airey, D., 2017. A spheropolygonal-based DEM study into breakage under repetitive compression. In: Proceedings of the EPJ Web of Conferences, 140. EDP Sciences, p. 7007.

Morrison, R.D., Cleary, P.W., 2004. Using DEM to model ore breakage within a pilot scale SAG mill. Miner. Eng. 17 (11–12), 1117–1124. doi:10.1016/j.mineng.2004.06.016.

Oda, M., 1982. Fabric tensor for discontinuous geological materials. Soils Found. 22 (4), 96–108.

Palmer, A.C., Sanderson, T.J.O., 1991. Fractal crushing of ice and brittle solids. Proc. R. Soc. A Math. Phys. Eng. Sci. 433 (1889), 469–477. doi:10.1098/rspa.1991.0060.

Ramkrishna, D., 2000. Population Balances Theory and Applications to Particulate Systems in Engineering, 1st Academic Press, San Diego doi:10.1016/B978-012576970-9/50007-2.

Sammis, C., King, G., Biegel, R., 1987. The kinematics of gouge deformation. Pure Appl. Geophys. PAGEOPH 125 (5), 777–812. doi:10.1007/BF00878033.

Sethna, J.P., 2011. Statistical Mechanics, Entropy, Order Parameters and Complexity, 2. Oxford University Press. 10.1.1.165.9961

Shi, Y., Sader, J.E., 1998. Lattice Boltzmann method for fluid flows. Annu. Rev. Fluid Mech. 30 (Kadanoff 1986), 329–364.

Turcotte, D.L., 1989. Fractals in geology and geophysics. Pure Appl. Geophys. PAGEOPH 131 (1), 171–196. doi:10.1007/BF00874486.

Weibull, W., 1951. Wide applicability. J. Appl. Mech. 103 (730), 293–297.

Yu, A., Standish, N., 1988. An analytical–parametric theory of the random packing of particles. Powder Technol. 55 (3), 171–186.

Zhang, X., Baudet, B., 2014. The multi-fractal nature of soil particle size distribution. Geomech. Micro Macro 1183–1188. doi:10.1201/b17395-213.

Zhang, Y., Buscarnera, G., 2017. A rate-dependent breakage model based on the kinetics of crack growth at the grain scale. Géotechnique 67 (11), 953–967.

Zhang, Y., Buscarnera, G., Einav, I., 2016. Grain size dependence of yielding in granular soils interpreted using fracture mechanics, breakage mechanics and Weibull statistics. Géotechnique 66 (2), 149–160.